DYNAMICS AND STRUCTURE OF THE OUTER RADIATION BELT

C.Y. Fan, et al.

The University of Chicago
Chicago, Illinois

September 1961

EFINS-61-34

DYNAMICS AND STRUCTURE OF THE OUTER RADIATION BELT*

By
C. Y. Fan‡, P. Meyer and J. A. Simpson
Enrico Fermi Institute for Nuclear Studies
University of Chicago
Chicago 37, Illinois

~~Submitted to the~~ /
Journal of Geophysical Research v. 66: 2607-2640 Sept 1961
~~June~~, ~~1961~~

*This research was supported in part by the National Aeronautics and Space Administration under Contract NASw-24, and in part by the Air Force Office of Scientific Research under Contract AF18 (600)-666.

‡Also Laboratories for Applied Sciences, University of Chicago, Chicago, Illinois.

DYNAMICS AND STRUCTURE OF THE OUTER RADIATION BELT

C. Y. Fan, P. Meyer and J. A. Simpson

ABSTRACT

From an analysis of electron measurements in the Explorer VI satellite (August 7 - October 6, 1959) four time-dependent parameters have been investigated which characterize the outer electron belt. They are: (1) the equatorial electron intensity I_o, (2) the equatorial range from the earth R_o of the peak intensity, (3) the electron density distribution along a line of force through the intensity peak, and (4) a measure of the change in electron spectrum with time. These parameters along with measurements of magnetic field intensity make it possible to study the origin of the changes in electron intensity and distribution which are known to occur in the outer belt. Several magnetic storms occurred during the observation on Explorer VI. Within the sequence of changes in the outer belt induced by these geomagnetic storms, there are some changes of the parameters which are accounted for only by invoking an irreversible energy gain or loss within the outer belt. The energy gain process appears to be through irreversible local acceleration of electrons. The energy loss process leads to a stable mirror point distribution characteristic of the periods between geomagnetic storms. The time intervals are identified within which each of these processes is operative. Reversible

processes are possibly the cause for other changes.

The foregoing analysis rests upon the proof given in this paper that the outer belt peak intensity coincides over a wide range of geomagnetic latitudes with magnetic field lines of force in the centered dipole approximation. Consequently, the measured electron intensity maximum is used as a "tracer" of the geomagnetic field lines of force for analyzing changes in the outer belt with time. It is shown that even during geomagnetic storms the trace of the electron intensity maximum followed a centered dipole line of force. This indicates that at all times the particle energy density of the radiation belt is much less than the energy density of the magnetic field in the region.

The electron fluxes, high energy proton fluxes and possible electron spectra are investigated. Two distinct peaks of electron intensity are identified to persist in the outer belt for about two months, and it is shown that these peak distributions undergo radial motion during geomagnetic disturbances.

I. INTRODUCTION

The first measurements of charged particles trapped within the geomagnetic field were made by the Iowa (Van Allen, McIlwain and Ludwig, 1959) and by the USSR groups (Vernov, Chudakov, Vakulov and Logachev, 1959a). Subsequent observations proved the existence of an inner belt composed of energetic protons and electrons, and an outer radiation belt dominated by energetic electrons. Single traversals of the outer belt made at different times led to the conclusion that the characteristics of this outer belt changed with time and solar activity. The origin of the inner belt protons is satisfactorily accounted for by the decay products of fast neutrons escaping from the terrestrial atmosphere. Although the origin of the outer belt at first was ascribed to electrons accelerated at the sun and subsequently trapped in the geomagnetic field, this hypothesis foundered both on the basis of physical principles, and through experimental evidence, including results reported in this present paper. Therefore, if electrons are to be introduced from the sun, or other sources at very low energy, it is required that they be accelerated in the geomagnetic field to yield the persistent, variable flux of energetic electrons observed in the outer radiation belt. On the other hand, if the outer belt electrons are ambient electrons, or electrons from neutron decay (Hess, 1960 ; Dessler and Karplus, 1960), then the changes in electron intensity and spatial distribution must also arise from magnetic field changes.

Therefore we conclude that a study of the changes in the electron outer belt brought about by changes in the geomagnetic field may lead us to the origin of these trapped electrons.

The energy which produces the variations of the external geomagnetic field comes from solar events, such as the solar flares, which emit ionized plasma leading to the classical geomagnetic storm.

There are a variety of ways by which some of these changes in energy and distribution of trapped electrons may be brought about (for example, Northrop and Teller 1960, Parker 1961a). Either rapid field changes including hydromagnetic wave propagation lead to the violation of one or more of the adiabatic invariants, and hence to <u>irreversible</u> acceleration or loss of energy in the belt, <u>or</u> slow field changes may dominate to produce <u>reversible</u> acceleration and consequent changes in the particle distributions in space.

The main purpose of the present investigation is to decide whether reversible processes determine the changing character of the outer electron belt, or irreversible processes must be invoked. The experiment, therefore, requires frequent, sequential traversals of the outer electron region at intermediate and low latitudes for extended periods of time under both quiet field conditions as well as during geomagnetic storms. An investigation of this kind was first undertaken by the Explorer VI satellite launched 7 August, 1959 in the highly elliptic orbit shown in Figure 1. This

satellite carried a group of charged particle radiation detectors having a wide dynamic range and variety of energy responses, as well as a magnetometer. The types of radiation detection instruments are given in Appendix 1, Table I along with a list of all space vehicles which at this writing have passed through the outer belt at low latitudes (Appendix I, Table II). The measurements were obtained under fortunate circumstances, since the geomagnetic field remained quiescent for a week before the commencement of two geomagnetic storms closely spaced in time. All of the data are within the period 7 August through 6 October, 1959, following which time the transmitter ceased to operate.

A preliminary account of our experiments (Fan, Meyer and Simpson, 1960) has shown several new properties of the trapped electrons in the outer belt, such as the persistent existence of a double belt structure in the outer zone and radial motions of these peak intensity distributions with time. We also observed the large scale time-dependent changes of intensity and particle distributions following geomagnetic storms which have also been reported by other investigators with apparatus on Explorer VI (Arnoldy, Hoffman and Winckler, 1960a) (Rosen, Farley and Sonett, 1960). However, our detailed study and conclusions regarding the outer belt electrons have awaited the full reduction of data, the availability of correlating solar geophysical data, and improved orbit calculations for Explorer VI.

To prove whether there exist irreversible changes or only reversible changes, our investigation centers on the identification and measurement of parameters which describe the characteristics of the outer belt and their changes with time. We first show that a centered dipole magnetic field is a good approximation for the description of trapped electron guiding centers in the outer belt, even during periods of geomagnetic storms. Thus, the positions of intensity maxima in the outer belt become "tracers" by which we follow changes in position, intensity, or other parameters as a function of time. It is then possible to follow systematically through the progress of a geomagnetic storm the changes of parameters such as the equatorial range R_o of the outer belt, or the equatorial intensity maximum I_o. To investigate reversible and irreversible processes we also need to know the electron mirror point distribution along a magnetic line of force and the changes in this distribution with time. Having proved that the centered dipole approximation describes the lines of force in space in the outer belt we are able to construct experimental curves of electron intensity as a function of position along magnetic lines of force and relate the changes in their distributions to geomagnetic storms.

The analysis of bremsstrahlung intensity rests upon some knowledge of the changes in electron spectrum with time and position in the geomagnetic field. Through the introduction of a parameter which reveals when the electron spectrum changes as a function of position or time we

separate spectral changes during magnetic storms from changes in mirror point distributions, etc. The measurements show that there is a concentration of electrons at the equator during some geomagnetic storms.

Our results lead to the identification of two irreversible processes among all the changes in the electron outer belt during geomagnetic storms. One is an energy or particle gain; the other is an energy or particle loss. Although not disproved, it also appears unlikely that the outer belt electrons are solar electrons which arrive with sub-detection energies to undergo local postacceleration. It is probable that the irreversible processes of gain and loss operate on ambient electrons and beta decay electrons. Some conditions are established for developing specific models of the electron outer belt.

II. CHARACTERISTICS OF THE DETECTOR SYSTEM

In order to separate high-energy protons ($>$ 75 Mev) and electrons (E $>$ 13 Mev) from bremsstrahlung produced by lower energy electrons, a triple coincidence telescope consisting of seven methane-argon filled gas counters was used for the detectors (Figure 2). These counters operated in the semiproportional range with a dead-time of 0.8 microsecond. This makes it possible to distinguish the cosmic ray flux from the trapped radiation in the outer radiation belt and to separate the bremsstrahlung production from energetic protons in the inner radiation belt. Groups of these

counters were combined as shown in Figure 2 to form a wide-angle, triple-coincidence counter telescope so that the accidental rate would be negligible even for the highest fluxes expected in the outer belt. The wide-angle was chosen to avoid the variation of counting rates due to any possible anisotropy of the radiation in the geomagnetic field. The lead shield surrounds the triple-coincidence telescope for two reasons. One, it provides a threshold for the minimum energy protons detectable by the triple-coincidence telescope (75 Mev for protons and $\geq$ 13 Mev for electrons). Two, the five grams-cm^{-2} of lead reduces the total counting rate in each of the individual counters to such a level that even for the highest fluxes attainable in the outer radiation belt, only minor corrections due to the dead-time were needed and were never more than 2% .

The information from the outputs of the two scalers in Figure 2 were transmitted to ground receiving stations through two subcarrier channels in the Explorer VI satellite.

The response of this detector system to protons was studied using the University of Chicago synchrocyclotron proton beam. The results are shown in Figure 3 for the detector axis perpendicular to the proton beam over an energy range of 50 to 250 Mev. In measuring relatively flat spectra like the cosmic radiation and the inner belt protons (Freden and White, 1960) this detector possesses a sharp cut-off at the mean energy of 100 Mev. For solar flare protons where the spectra may be as steep as $1/E^5$, the gradual change in

sensitivity in the region from 75 to 100 Mev, as shown in Figure 3, must be taken into account.

The noncoincident high counting rates of the single counter during the passage through the outer belt must be due exclusively to geomagnetically trapped electrons which produce bremsstrahlung either in the satellite shell, interior objects, or in the surrounding lead shield. With an unknown energy spectrum it is obviously impossible to relate the count rate of the single counter to the flux of particles or energy flux carried by the electrons incident on the vehicle. However, with proper calibration, we shall show in Section XI that significant limits on the particle flux and on the particle energy spectra may be derived.

The response of this bremsstrahlung detector to monoenergetic electrons was studied in the laboratory using the electron beam from Van de Graaff generators (High-Voltage Engineering Co. and the General Electric Co.), and a low energy X-ray source at the University of Minnesota. The completely assembled spare payload of Explorer VI, with a mass distribution identical to the flight unit, was mounted so that it could be rotated about two mutually perpendicular axes for exposing any portion of its surface to direct electron bombardment. (The electron flux in the energy range from 250 Kev to 1 Mev in discrete energy intervals irradiated the payload from various directions so that an averaged response of the counter for isotropic radiation could be deduced. This experiment differs from an exposure

to particles in space in two ways: 1) There was air present inside the payload; and 2) the electron beam for each exposure was unidirectional instead of omnidirectional. Additional measurements were obtained inside the vacuum system using the bremsstrahlung detector with an absorber simulating the satellite shell.)

Since the shell of Explorer VI payload is made of aluminum 170 mg/cm^2 thick, all electrons with energies below 500 Kev are stopped in the shell. Therefore the response of our radiation detector to electrons below 500 Kev is due entirely to bremsstrahlung produced in the payload shell. This was verified by showing that the count rate for an equivalent electron flux was proportional to the inverse square of the distance between the detector and the irradiated area on the shell. The angular distribution of X-rays within the satellite appears to be sufficiently isotropic to use the inverse square law for those parts of the payload where no appreciable absorption material is located between the satellite shell and our detector. The assumption of isotropy for the X-rays produced in the shell will be an even better approximation in the actual case of omnidirectional incidence of electrons in space.

For the equatorial plane of the vehicle where the instruments and associated equipment are located the experimental count rates for the electron flux incident at various payload longitudes were used to compute the bremsstrahlung contribution. The openings between equipment and electronic

parts in the payload were studied and the calibration takes into account factors which could influence the count rate from low energy X-rays.

From these measurements we wish to obtain the flux of monoenergetic electrons isotropically incident upon the satellite from the counting rate of our bremsstrahlung detector. To this end we integrated over the response curve in the equatorial plane and added the upper and lower hemisphere integrations of the payload shell separately. Thus we obtained the response curve in counting rate per electron per cm^2 bombarding the shell as shown in Figure 4. The portion of the curve between 200 Kev and 1000 Kev can be expressed as a power law $E^{4.7}$.

The performance of our detector system for separating trapped protons and cosmic radiation from bremsstrahlung is clearly shown in the Explorer VI measurements of Figure 5 which represents a traversal through the inner and outer radiation belts at high geomagnetic latitudes.* The triple-coincidence counting rate rises to a maximum value at 8500 Km representing the peak of the inner radiation belt for protons $>$ 100 Mev, and decreases to a cosmic ray background at the radial distance of 9500 Km and beyond.

---

* During each period of satellite motion there are two passes through the Van Allen belts - we define an ingoing or outgoing traversal of the trapped radiation as a pass, numbered consecutively from launch. The dates of the consecutively numbered passes are given in Appendix I, Table III.

For counting penetrating particles the calculated omnidirectional cross-section is 5.5 cm^2 which is 1.95 times the cross-section for triple-coincidences measured with Explorer VI, and 1.93 with Pioneer V. These measurements were obtained using the omnidirectional cosmic ray intensity at great distances from the earth with no bremsstrahlung present. Any increase in this ratio signifies bremsstrahlung detected by the single counter. For example, in the outer belt the bremsstrahlung rate reaches 1.8 x 10^4 counts/sec compared with a triples count rate of 5 to 6 counts/sec. from cosmic radiation. In Figure 5 it is seen that detectible bremsstrahlung sets in on the outer slope of the inner radiation belt and increases until reaching a peak intensity of the outer belt. These measurements demonstrate the separation of the detection of bremsstrahlung from energetic nucleonic particles. It is also interesting to note that the triple coincidence detector has measured untrapped solar flare protons while it was in the outer radiation belt where the highest singles count rate was 6,500 counts/sec. (Fan, Meyer and Simpson, 1960).

III. THE EXISTENCE OF TWO ELECTRON INTENSITY PEAKS

Typical data recorded during passes through the trapped radiation regions are shown in Figure 6 and Figures 7a and 7b. They immediately reveal the existence of the two electron intensity peaks which were reported in 1959

(Fan, Meyer and Simpson, 1960). Using an ion chamber and Geiger counter, the Minnesota group have confirmed the existence of this double electron peak structure (Arnoldy, Hoffman and Winckler, 1960b). Since our data show throughout the eight weeks of Explorer VI recordings that a double peak is a persistent characteristic, and since a re-evaluation of earlier space shot data suggests the possible existence of this intermediate range peak even over greater periods of time, we suggest that two separated electron intensity maxima may be a persistent feature of the outer radiation belt. We, therefore, use in this paper the nomenclature, proposed earlier, designating with the subscripts 1, 2, 3 the peak intensities at successive radial distance and indicating by letter P or E whether we observe protons or electrons, i.e. the electron regions E_2 and E_3 are the outer Van Allen belt, thus the maxima in Figure 6 are identified as P_1, E_2 and E_3.

The two peaks in Figures 7a and 7b lie in the E_2 and E_3 regions. To reduce the Explorer VI observations to a quantitative study, it is necessary to trace the identity of these regions through intensity changes or positional changes of the outer belt with time before, during or after geomagnetic disturbances. Therefore, we have defined the <u>maximum</u> intensity of E_2 and the <u>maximum</u> intensity of E_3 as "signatures" of the E_2 and E_3 regions, and we use these maxima to trace the E_2 and E_3 electron distributions in the geomagnetic field both in space and time. For

example, for a given peak distribution at the equator during times of quiescent geomagnetic field, the peak intensity is to be assigned to a magnetic line of force of the dipole field at range R_o as we show in the next section. With the assumptions that the guiding center approximation holds for the trapped electrons and that both the energy spectrum and the pitch angle distribution do not drastically change in the neighborhood of the line of force through E_3 (max), we find that the maximum intensity of the electrons will be along a line of force over the entire range of latitudes for which the radiation is trapped (Fan, Meyer and Simpson, 1961). Thus, we may use the position of maximum intensity to give us the trace in the meridian plane of the geomagnetic line of force passing through E_3 (max) or E_2 (max).

IV. THE GEOMAGNETIC FIELD AND THE REPRESENTATION OF EXPLORER VI ORBIT

Since the magnetic field of the earth is described by a dipole inclined with respect to the rotation axis, plus higher order terms, and the period of the satellite is approximately 12.7 hours, the satellite successively passes through different portions of the magnetic field in its motion about the earth, only returning to its initial position with respect to geomagnetic coordinates after approximately 32 satellite passes. For studies of the outer radiation belt where the range R (distance from dipole to satellite) is the order of 15×10^3 to 30×10^3 Km. or more,

we can neglect the higher order terms. The best test for the validity of this approximation is found in the consistency with which data obtained in the outer radiation belt fit together smoothly with the dipole approximation over a wide range of geomagnetic coordinates and at different times. This is shown as follows:

In Figure 8 we plot the positions of E_3 (max) in R_o, $\cos^2\lambda$ coordinates for which the line of force in the center dipole approximation becomes a straight line passing through the origin. The data used were obtained in a short time interval since we find that the position of the intensity maximum changes with time. The high latitude data have been corrected according to Appendix II. Within the limits of experimental errors which we believe to be $\pm$ 300 Km. the data lie on straight lines. The data for August 21 were obtained during magnetic disturbances (Figure 13) when the intensity was changing by a large factor. Hence, we conclude that the centered dipole approximation is valid in the outer radiation belt not only for the undisturbed field but also during times of geomagnetic disturbances. This result has been shown in our earlier report (Fan, Meyer and Simpson, 1960). The important implication of the alignment of E_3 (max) with undistorted dipole lines of force is the energy density ρ_e at all times must be less than the magnetic field energy density ρ_m in the outer radiation belt (for otherwise the magnetic field line would have been distorted by the presence of the particles).

Thus the problem reduces to the description of the satellite motion in the geomagnetic dipole meridian plane -- a representation used also by other investigators in the description of satellite and space probe measurements. Figure 9 shows typical trajectories in the λ-R plane and indicates how, over an extended period of time, large volumes of space in the vicinity of the trapped radiation are covered by the Explorer VI orbit.

However, we wish to point out another representation for the orbit trajectory (Fan, Meyer and Simpson, 1961). If the dipole approximation is valid for outer belt analysis as we have claimed, then the geomagnetic field lines are described by the equation $R = R_o \cos^2\lambda$, where λ is the geomagnetic latitude and R_o the equatorial distance of a line of force from the center of the dipole. Lines of force with range R_o around the earth are equivalent (azimuthal symmetry). Thus, the orbit may be described on a plane R_o vs. R wherein each field line becomes a horizontal line in the two-dimensional plot. Trajectory data in these coordinates are shown in Figure 10. We see that a significant portion of the satellite motion may be projected onto a single dipole line of force whose range at the equator is R_o'. Since the electron intensity is measured continuously we may obtain curves for intensity as a function of λ (or magnetic field intensity) along a line of force as shown in Section VII. If we allow a range spread of about 200 Km. then we obtain useful data of

this type from over one-third of all Explorer VI trajectory passes. Among these passes we find many which lie on the same R_o as the position of E_3 (maximum).

In Section VII it will be shown that the intensity along a line of force near E_3 (maximum) changes rapidly with λ. Also, we note from Figure 9 that the satellite sometimes moves obliquely across the region of E_3 (max) where the intensity is a strong function of latitude and range. For such cases the observed position of electron intensity peak and the true position of intensity maximum are in general different. This problem is discussed in Appendix II. The problem is restricted to high latitudes, since at low latitudes the traversals are always at a large angle with respect to the lines of force. From Appendix II it is clear that corrections in range and latitude are significant in locating the true position of E_3 (max) at high latitudes. We have applied these corrections in the region of E_3 (max) in this paper.

In Figure 11 the positions of the maxima for regions E_2 and E_3 are plotted in the meridian plane for a large number of trajectory passes. This is an extension of results already published (Fan, Meyer and Simpson, 1960). From Figure 11 it is clear that the two maxima lie along lines of force and retain their separate identity to very high latitudes. It is also clear that the intensity minimum between E_2 and E_3 in the outer belt is not the "gap" described in the literature between the inner and outer belts.

V. THE RADIAL CHANGE OF ELECTRON BELTS

To investigate in greater detail the radial motion of the two electron belts as a function of time which is evident from Figure 11 we have used all passes through E_2 and E_3 with the criterion for identification of maxima outlined in Appendix II. We then determined the equivalent equatorial range R_o of the magnetic dipole line of force on which each maximum was found to lie. The results of this extrapolation appear in Figure 12. Since systematic and progressive errors in the time - position data of the satellite trajectory could introduce "drifts", we have investigated the question of the accuracy of the orbital data, especially with respect to variable atmospheric drag at perigee. Although we know there are errors between the calculated and real positions of the satellite at small range -- serious for inner belt studies -- the errors in the outer region until at least September 9 are 500 - 100 Km. in range. (See Appendix II.) It is reassuring to note that after pass 67, on September 12 the U.S.S.R. second cosmic rocket data showed a principal maximum in the outer electron belt at the same position measured with our Explorer VI detector for region E_3 (max) on September 13 (Vernov and Chudakov, 1960). Consequently, the large changes of range in Figure 12 represent real changes of the intensity maxima with time and lead to the conclusions:

1) There exist rapid and simultaneous changes in range of E_3 (max) and E_2 (max) during geomagnetic

storms. The magnitude of the change may be as great as 10% of the total range from the dipole center.

2) Both regions tend to undergo the same inward direction of motion with the magnitude of change being much less for E_2.

Whether outward motion occurs depends upon the interpretation placed on the data after the geomagnetic storm on 3 September. Unfortunately the ground stations were closed for a few days. We have indicated by arrows the alternate interpretations which may be placed on the data after September 3. Two regions continue to persist but their identities become obscure. The maximum appearing beyond 27,000 Km. after September 25 might be interpretated as either a new region forming and moving inward or a shift in the previous E_3 (max). In any case, inward motion is certain at some times, outward motion is not excluded at other times by our results.

The physical explanation for these radial motions of the outer belt is unclear. If, as appears likely, the motions are mainly inward then drift or diffusion across lines of force might seem to be an attractive explanation, especially since the drift occurred during a geomagnetic disturbance. Although inward motion of electrons in non-uniform magnetic fields is a well-recognized possibility (Herlofson, 1960; Parker, 1961a), both the short time constants and the persistence of a "sharp" maximum with

high intensity at all times in the experimental data argue against inward diffusion.

The changes have the gross appearance of lines of force moving inward as though the scale of the dipole were decreasing. It has been argued that as a consequence of the insulating shell of the earth lines of force may be progressively brought inward (Gold, 1959). However, the peak distribution would rapidly disappear, contrary to fact.

The Argus experiment (Van Allen, McIlwain and Ludwig, 1959b) showed that the intensity maximum of trapped β-rays from fission products did not change radially during the entire period of observation by more than $\sim$ 30 Km. even though geomagnetic disturbances were taking place. Since the ranges of the Argus "shells" were less than for region E_2, the radial motion we have found presumably has its origin in magnetic field and current system changes beyond the range of E_2 and E_3 at the times of geomagnetic storms.

VI. INTENSITY CHANGES OF E_2 AND E_3 REGIONS WITH TIME

Since the satellite trajectories cover a wide range of geomagnetic latitudes as a function of time, the spatial distribution and changes with time of the intensities are intermixed. We shall first consider exclusively the data obtained in an equatorial band of latitudes $\pm 10^{\circ}$ for which case the spatial variation may be neglected. We shall then

extend this analysis to higher geomagnetic latitudes, and finally to a description of the intensity along a magnetic line of force as a function of time.

The results for intensity changes in the equatorial plane are shown in Figure 13 for the region E_3. For the first seven days after launch the intensity is constant within the accuracy of the measurements. Thereafter large intensity variations occurred in association with geomagnetic storms. On August 16, a severe geomagnetic storm began with sudden commencement at 0400 UT. The magnitude of the changes in the equatorial horizontal component of the geomagnetic field at the surface of the earth is plotted in Figure 13A. The magnetic field in the outer belt was also measured at this time. Figure 13B (Smith and Rosen, 1960; Smith and Sonnet, 1961). The period of violent magnetic disturbances, represented by large values of A_p, continued into August 17 - 18. Since it is well known that more than 7 - 10 days are required for the field to return to its normal condition, the second sudden commencement magnetic storm which began at 0410 U.T. August 20 must have been superposed on the recovery phase of the August 16 storm. The August 20 storm was coincident with a sudden decrease of $\sim$ 15% of cosmic ray intensity in space. (Fan, Meyer and Simpson, 1960).

Gross changes of intensity in the E_3 region have also been observed with the other radiation detectors on Explorer VI. (Arnoldy, Hoffman and Winckler, 1960a, 1960b; Rosen

Farley and Sonett, 1960). The most obvious phenomena we note are a sudden decrease of intensity following the initial phase of the storm, and later, a buildup by a factor 3 in intensity within 24 hours during the main phase and recovery of the first storm. The equatorial peak intensity increased by another factor $\sim$ 3 at the time of the second magnetic storm on 20 August. The intensity then gradually declines, and after the magnetic storm of September 3, reaches approximately the values obtained at the time of launch. We note here that geomagnetic storms occurred also on 20 September and 3 October. These latter two storms were minor compared with the events of August 16 and 20.

We now investigate the intensity changes with time at higher geomagnetic latitudes, viz. at higher field intensities along lines of force through E_3 (max). Since the intensity decreases rapidly with increasing latitude, curves similar to Figure 13 at higher latitudes can only be obtained by using data from small intervals of latitude. Therefore, all data in the latitude intervals $\lambda = 20^\circ \pm 10^\circ$ and $40^\circ \pm 10^\circ$ were interpolated (Section VII) to 20° and 40°, respectively and are shown in Figure 14. These curves for 0°, 20° and 40° reflect the changes of electron pitch-angles with time. We discuss quantitatively the physical meaning of these observations after examining the detailed electron intensity distribution along a line of force.

VII. THE ELECTRON INTENSITY ALONG LINES OF FORCE AS A FUNCTION OF TIME.

From the electron density measured along a tube of force either the distribution of mirror points or the equatorial pitch angle distribution of electrons may be determined. Thus, these measurements are fundamental to an understanding of the electron source and loss mechanisms in the outer belt.

We note from Section IV, Figure 10, that for some passes the satellite moved along a dipole line of force for a significant interval of time and that approximately one-third of all passes contained data of this kind. Curves for Intensity I vs λ have been constructed by supplementing these passes with individual crossings of the same force line at different latitudes but at closely related times.

We first show in Figure 15 the intensity along a line of force passing through the maximum of E_3 during times when the geomagnetic field is relatively quiet. Curve A is for a period before the geomagnetic storms, and Curve B represents a quiet period* where the counting rate was still high following the geomagnetic storms.

All additional data along segments of lines of force, not necessarily through E_3 (max), are given in Figure 16 for both magnetically quiet and geomagnetic storm periods.

*The lowest magnetic disturbance indices for August and September occurred on August 26.

We have found that all these data, to a good approximation, may be represented by

$$\frac{I}{I_0} = \left(\frac{B}{B_0}\right)^{-x} \qquad (1)$$

at intermediate latitudes, and, for periods free from magnetic storms, even to the equator. The symbols I_0 and B_0 refer to equatorial electron and magnetic field intensity, respectively.

The data from Figures 15 and 16 have been plotted in Figures 17 and 18 using expression (1) and a dipole magnetic field for those cases where the lines of force passed through E_3 (max). The values of the exponent x for these curves are listed in Table I.

Provided there are no large changes in the electron spectrum with time along a line of force through E_3 (max), a condition we later show to be satisfied (Section VIII, Figure 21) then the curves in Figure 17 prove that the pitch angle distribution (or mirror points) is changed during the main phase of the first geomagnetic storm. The relationship between the exponent x and equatorial pitch angle distribution has been discussed recently (Fan, Meyer and Simpson, 1961). Figure 17 also proves that the particle intensity increase is initially concentrated at the equator, and only at a later time in the development of the magnetic storm does the electron flux at large B/B_0 (high latitude) begin to rise.

In the same way we investigate the region E_2. Unfortunately, due to the high latitudes of the trajectory through the region of E_2 maximum, there are only individual points and no sections of data along lines of force. Therefore, we must be content with constructing the intensity along tubes of force using data, grouped over a period of several days. Since we showed (Fan, Meyer and Simpson, 1960) that the region E_2 is relatively immune to the large scale solar-induced phenomena associated with E_3, we use data over intervals of time for which there was negligible change in range R_o for E_2. These time intervals A_2, B_2, C_2, D_2 are given in Figure 19. The assumption that the spectrum is independent of latitude no longer holds for region E_2 as we shall show in Section VIII. Hence, we must confine our attention only to the relatively large scale changes in slope of the curves with time. The electron intensities along lines of force are shown in Figure 19 where the steep slope of curve B_2 corresponds to the time August 17 - 18 of the first geomagnetic storm. We conclude that during this phase of the storm the mean pitch angle of electrons in region E_2 also increased.

VIII. CHANGES IN ELECTRON ENERGY SPECTRUM WITH RANGE, LATITUDE AND TIME

The analysis of the outer belt electrons has so far provided us with the time dependent parameters of electron intensity I, equatorial range R_o of E_3 (max), and a function x representing the electron pitch angle,

or mirror point, distribution along a line of force. Since the electron flux is measured by its bremsstrahlung produced in the satellite it is essential also to understand the major changes which may take place in the spectrum of trapped electrons during and after the magnetic storm. For example, if the spectrum of electrons changed along a line of force in such a way that the mean energy is much higher near the equator than at high latitudes during the magnetic storm (for example, during Pass 22) it could not be argued that the observed increase in x (Figure 17) was due to an increased concentration of particles at the geomagnetic equator.

We approach this problem of spectral change with time and position as follows. Although we do not know the electron spectrum we can determine if there are changes in the spectrum by observing the relative change in count rates of two bremsstrahlung detectors, each having a different response to the electron spectrum. Two detectors suitable for this purpose are the G. M. counter of the Minnesota Group (Arnoldy, Hoffman and Winckler, 1960b), and the single, lead-shielded proportional counter.

Therefore, we use the change in the ratio $Z = \frac{\text{G. M. Count rate}}{\text{Proportional Count rate}}$ as an indicator of changes in the trapped electron spectrum.

The ratio Z is shown in Figure 20 as a function of equatorial range R_0 in 5° intervals of latitude. It decreases with increasing range R_0 but levels off at approximately

22,000 Km. Thus, the electron spectrum at high latitudes and small range is quite different from the spectrum at E_3 (max). Beyond 22,000 Km. there is a negligible change in spectrum.

These conclusions are verified in Figure 21, where we have plotted Z along selected lines of force. Pass 33 lies in the E_2 region. The data for Pass 22 were obtained during the intense magnetic storm, thus proving that the intensity changes along the line of force in Figure 17 are <u>not</u> due to changes in electron spectrum with latitude.

To isolate gross spectral changes with time from these spatial changes, we have selected only values of the ratio at E_3 (max) in the equatorial zone. This ratio is plotted in Figure 22 as a function of the single proportional counter intensity. We note here that:

a) There are no significant changes in spectrum until after reaching maximum intensity at Pass 25.

b) After Pass 25 there is a systematic change of spectrum for many days (even though some of the variations in ratio may be due to changes in range, etc.)

These results reveal that the electron spectra for Curves A and B in Figure 17 were different.

The above analysis did not depend upon assumptions regarding the form of the electron spectrum. If we assume, due to lack of detailed information that the

electron spectrum is given by $N(E)dE = AE^{-\gamma} dE$, then we may predict specific changes in the energy spectrum. This has been done in Appendix III where the value of γ is derived from the count-rate ratios and the detector response curves.

IX. THE ORIGIN OF CHANGES IN THE OUTER ELECTRON BELT

In the preceding sections of this paper we have established four parameters to represent the physical characteristics and changes with time of the outer electron belt; namely, 1) the maximum electron intensity at the equator I_o; 2) the mirror point distribution along a line of force represented by the exponent x; 3) the equatorial range of the dipole line of force passing through the principal maximum E_3 (max) of the outer belt R_o; and 4) the ratio Z which is sensitive to changes in the electron spectrum. All of these parameters possess spatial and time dependent characteristics.

We now investigate the basic question of the origin for changes in these parameters with time. It is clear that the time dependence originates with events at the sun which transport energy by means of plasma, radiation or particles to induce geomagnetic storms. It is not settled, however, whether the outer belt electrons have a long trapping time and undergo changes in energy and trajectory through variations of the geomagnetic field in such a way that when the field returns to its initial conditions, so

will the parameters of the trapped electrons. Is the origin of the changes with time to be found entirely in reversible processes, for example, the betatron effect? Or, are we forced to conclude that at least part of the effect is brought about by particle loss, local electron acceleration or injection, and, therefore, are we required to admit that irreversible processes are prominent in the changing character of the outer electron radiation belt?

In this section we shall show how the analysis of the four parameters I_o, R_o, x, Z along with a gross knowledge of the form of the time changes in geomagnetic field B enable us to decide between these alternatives.

First, we bring together in Figure 23 the main results of our analysis in earlier sections for the period before, during and after the two geomagnetic storms on August 16 and 20. This interval of time was chosen because of the large scale effects, and the availability of large amounts of data.

Second, our analysis is restricted to the region E_3 where the position of the maximum intensity in the dipole field is used as a "tracer" to follow the electron distribution with time. When we state that a particle distribution remains on a line of force through R_o we are using this line of force as representative of all lines of force around the earth at range R_o across which these particles drift with time. We have assumed the

centered dipole approximation where the field shape is independent of longitude.

Third, since the intensity changes of the geomagnetic field were measured in the E_3 region by the magnetometer on Explorer VI as shown in Figure 13B, we call attention here to the conclusion, important for the analysis which follows, that the magnetic field changes at the location of the E_3 region and at the surface of the earth (see Figure 13A) are similar -- especially with respect to the sign of the change in intensity with time. We also note that significant deviations of the magnetic field from the dipole approximation do not appear in the Explorer VI magnetometer records during the magnetic storms until ranges in excess of 25,000 Km are reached (Sonett, Smith, Judge and Coleman, Jr., 1960).

From Figures 13 and 23 we divide into eight successive time intervals the major changes in the outer radiation belt and relate them to the physical properties of the belt and the magnetic field.

Period t_1
(Aug. 7-15) This is the prestorm period where the mirror point distribution was constant and the intensity changed by less than 1% per day for the order of 7 days.

$$I_o(t_1) \approx \text{constant}$$
$$x(t_1) = 0.57$$

$R_o(t_1) \approx$ 23,000 Km.

$Z(t_1) \approx$ constant

These represent the initial conditions for our analysis.

Period t_2
Aug. 16-17

The sudden commencement of a magnetic storm occurred at 0405 U. T. August 16. Our first data after that time were obtained on Pass 19 (August 17) during the main (depressed intensity) phase of the magnetic storm. The magnetic disturbance index A_p was high throughout this period of time.

$I_o(t_2) \approx \frac{I_o(t_1)}{3}$

$x(t_2)$ unknown

$R_o(t_2) \approx$ 22,000 Km.

$Z(t_2) \approx Z(t_1)$ (negligible spectrum change)

We conclude that the changes between t_1 and t_2 could be explained by betatron deceleration*

Period t_3
Aug. 17-18

The magnetic field intensity at both the earth and at the region of E_3 (max) had rapidly returned to within ~ 0.6 of its prestorm value for Pass 21 on August 18. The magnetic disturbance index A_p was still high.

---

* The S.T.L. scintillation detector count rate increased at this time. We discuss this increase in Section XII.

$$I_o(t_3) \lessapprox 2\, I_o(t_1)$$

$$x = 1.2$$

$$R_o(t_3) \lessapprox R_o(t_1)$$

$$Z(t_3) \lessapprox Z(t_1)$$

Since (1) the range R_o of E_3 (max) was the same as before the storm, (2) the magnetic field has remained undistorted and (3) the field intensity was still below the prestorm value, the increase of I_o at t_3 by a factor $>$ 2 above $I_o(t_1)$ can only be explained by some irreversible process. In fact not only is $I_o(t_3) > I_o(t_1)$ but also $x(t_3) > x(t_1)$.

Period t_4
Aug.18-19

The magnetic field continues slowly to increase towards normal intensity on Pass 23. The electron flux is increasing and a flux appears at great distances ($>$ 40,000 Km) as shown in Section X.

$$I_o(t_4) \lessapprox 3\, I_o(t_1)$$

$$x \lessapprox 1$$

$$R_o(t_4) = R_o(t_1)$$

$$Z(t_4) = Z(t_1)$$

This step could be possibly accounted for by betatron effect.

Period t_5
Aug. 20

The second magnetic storm with sudden commencement at 0410 U.T. August 20 was followed within four hours by pass 25.

$$I_o(t_5) \approx 6\, I_o(t_1)$$

$$R_o(t_5) - R_o(t_4) \approx -2000 \text{ Km.}$$

$$x \succ 1$$

$$Z(t_5) \approx Z(t_1)$$

We could account for the flux increase as a reversible process if the field increase comes about through the change in range of 2000 Km for E_3 (max). Note the high concentration of electrons confined to within $\pm 15^\circ$ of the geomagnetic equator at this time.

Period t_6
Aug. 21-26

Between t_5 and t_6 there are the following changes:

$$I_o(t_6) \approx 4\, I_o(t_1)$$

$$\approx 2/3\, I_o(t_5)$$

$$x(t_6) = 0.6\ x(t_1)$$

$$R_o(t_6) \approx R_o(t_5)$$

$$Z(t_6) \succ Z(t_1)$$ (This significant change of the spectrum* is independent of latitude.)

The measurements for Curve B centered in time on August 26 are for a period of magnetically quiet days even though the magnetic field intensity at E_3 (max) was still below prestorm

---

*See Appendix III for probable form of spectrum change.

level. Note that the data suggest a lowering of mirror points and increase in flux at high latitudes even though the field strength in this region continued to increase.

Period t_7
Aug. 26-30

$$I_o(t_7) = 2\, I_o(t_1)$$
$$R_o(t_7) \approx R_o(t_1)$$
$$x(t_7) = x(t_6) = x(t_1)$$
$$Z(t_7) \approx Z(t_6)$$

We find here a reduction of intensity by a factor of ~ 2 without a significant change in the pitchangle distribution and the spectrum.

Period t_8
Sept. 3

The magnetic storm of September 3 with sudden commencement at 2200 U.T. was followed by high A_p values and resulted in a rapid return of I_o to the value $I_o(t_1)$ without a significant change in x as seen in Figure 16.

$$I_o(t_8) \cong I(t_1)$$
$$x(t_8) = x(t_1)$$
$$R_o(t_8) = \text{uncertain}$$
$$Z(t_8) \geq Z(t_7)$$

It is difficult to prove experimentally that a process is reversible because so much must be known about both the particle and magnetic field parameters. For example, Parker (Parker, 1961b) recently has shown that the

superposition of two deformations of the geomagnetic field can approximate almost any variation of electron distribution which maintains a "bell-shaped" latitude dependence. Parker finds three adjustable parameters are required to describe the possible reversible changes in a slowly changing geomagnetic field: namely T(t) which determines the magnitude of the field B_o, a(t) giving the scale of the field, and $\nu(t)$ describing the form of the field lines. Accordingly, wherever we stated that a given step could be explained as a reversible process, we imply the possibility of invoking changes in these magnetic field parameters to reconstruct the observed change in electron distribution.

The changes occurring between some of the eight periods above may be reversible. However, there are some changes which, under any model for trapped particles, could not be explained by reversible processes. Indeed, we need only prove that one of the series of changes is irreversible, and we prove the process as a whole to be an irreversible effect. For this test we choose first the change from period t_1 to period t_3.

We note that between t_1 and t_3 the magnitude of B decreased (T(t) was decreased) while both the dipole character of the field lines and the range of the field line through E_3 (max) were preserved (a(t) and $\nu(t)$ constant). Yet the electron density at t_3 was everywhere greater than at t_1. This change in the radiation belt had its origin either in an increase in energy of the already trapped

electrons, or additional particles have been added in the energy range to which the detectors are sensitive.

What irreversible process could bring about this result? Briefly, there exist two extreme alternatives:

a) If, at period t_2 during the main phase of the geomagnetic storm with the total field intensity at its minimum value, electrons are injected somehow with energies below the detection level of the bremsstrahlung detectors then when the field recovers to $\sim$ 0.6 of its initial value these new particles could be brought up to energies where they produce bremsstrahlung with increased efficiency. However, this explanation is unlikely since it is required to preserve the ratio Z (or the spectrum) and the new particles would have to be concentrated about E_3 (max) to preserve the range of E_3 (max).

b) During the period t_2 of the storm's main phase there were small scale but rapid magnetic field intensity variations (high A_p) which could be invoked through some irreversible process to accelerate electrons. Such an unspecified process plus the partial recovery of over-all field intensity could not only bring the intensity above its prestorm value but also increase the electron density near to the equator.

We do not attempt here to build models for the observed irreversibility but only emphasize that the existence of this step removes the possibility for a reversible theory of outer belt intensity variations.

Another irreversible step clearly exists between t_5 and t_6. On the basis of equatorial data the magnetic field intensity increases while the changing electron distribution remains along a dipole line of force of constant R_o. The evidence is against any change in scale of the field. The electron mirror point distribution returned to nearly the prestorm values which is equivalent to the equatorial intensity declining while the high latitude intensity increased. These changes were accompanied by a change in energy spectrum. If we assume that the spectrum was of the form $E^{-\gamma}$ then we observed an increase in γ. These changes reveal an irreversible loss of particle energy, or particles. The data indicate a relative loss of particles at high energy which could come about either by the escape of high energy particles or a radiative energy loss at high energy. A similar irreversible process is found between t_6 and t_7.

Thus our investigation has led us to two irreversible processes, one an irreversible energy gain and the other an irreversible loss. At present we do not understand either of the underlying phenomena.

X. The Electron Fluxes Beyond the Outer Belt

At ranges greater than 40,000 Km (corresponding to lines of force reaching the earth at geomagnetic latitudes greater than 67°) the proportional counter normally detects only the cosmic ray flux. Therefore, we may invoke a hypothetical, spherical surface with radius of 40,000 Km to surround the trapped radiation and determine the fluxes of high energy electrons, if any, which are trapped or pass through this "boundary" from time to time. We do this by plotting in Figure 24 the single count rate for all data at distances greater than 40,000 Km. as a function of time. As shown in Section II, this count rate is the sum of the omnidirectional cosmic ray intensity, normally 9.5 counts/sec., and any bremsstrahlung produced by electrons. The singles count rate for the cosmic radiation exhibited three successive Forbush type intensity decreases, as shown by the arrows in Figure 24. Thus, the excess count rate over approximately 10 counts/sec. is due to bremsstrahlung by electrons incident on Explorer VI. One single count indicates an omnidirectional intensity of 3×10^6 electrons/sec/cm^2 if the energy is 200 Kev. We note that in addition to low level fluctuations (less than 1 count/sec.) there exist occasional outstanding bursts, especially the increase on August 19, which would represent a flux of 9×10^6 electrons/sec.-cm^2 for 200 Kev. electrons.

The scintillation counter detected rapid intensity fluctuations correlated with magnetometer fluctuations in

the same regions of space (Farley and Rosen, 1960). These electrons must be trapped.

Since these electrons appeared during the period of intensity buildup in region E_3 it is tempting to assume that the flux represents the arrival of solar electrons, which diffuse inward in the equatorial magnetic field. However, they could not be preaccelerated electrons which find their way into the E_3 region for the purpose of producing the many-fold increase of equatorial intensity because: 1) the E_3 intensity buildup began (between periods t_2 and t_3) many hours before this distant flux reached a high level and only after the kind of field fluctuations which might allow trapping had subsided; 2) there is no a priori mechanism whereby the process of trapping new particles should preserve the location of E_3 (max), or the energy spectrum; and 3) as a precondition for trapping, the incoming particle density must approximate the trapped particle density; but, on August 18 - 19 the flux was several orders of magnitude lower than required.

However, the possibilities exist that these particles are "spillage" from the auroral zone, or that they have drifted outward from the equator as a result of instabilities* during the rapid buildup of E_3 (max) intensity.

---

* For example, the recently studied velocity-space instability observed in mirror machine geometries by R. F. Post. (Private communication from R. F. Post to J.A.S. (R. F. Post and W. A. Perkins, 1961).

XI. Electron Flux, Energy Density and Spectrum

Bremsstrahlung measurements do not give directly the electron flux and energy spectrum. Therefore, we shall assume an energy spectrum and compute the electron flux from the single counter count rate and response curve in Figure 4 for monoenergetic electrons. For any assumed energy spectrum, we have the additional boundary condition that the energy density of the geomagnetic field ρ_m, at any point must considerably exceed the electron energy density ρ_e at that point. This condition was proved in Section IV for both normal and disturbed geomagnetic field conditions. This boundary condition, $\rho_m > \rho_e$, is most severe in the limiting case of the geomagnetic equator at the range of maximum E_3 intensity, where the electron density is highest and the field energy density is lowest along the line of force passing through E_3 (max). For the quiet period prior to 14 August, 1959 where E_3 (max) lies at approximately 22 to 23 x 10^3 km, we find for an undisturbed dipole field a magnetic field energy density of $\approx$ 2 x 10^{-6} erg/cm^3.

Experimental evidence on the electron spectrum is scarce. The only direct measurements (Walt, Chase, Cladis, Imhof and Knecht, 1960; Cladis, Chase, Imhof and Knecht, 1961) were carried out at low altitude ($\approx$ 1000 Km) along a line of force passing through the geomagnetic equator at a range of $\approx$ 9000 Km. and, therefore, far below the range of E_2 (max).

In the energy range accessible to our detectors their data are consistent with a differential energy spectrum of the form $N(E)\,dE = AE^{-\gamma}\,dE$ with $4 < \gamma < 5$. This exponent agrees with the analysis of the ratio of G. M. and proportional counters for a range less than the range of E_2 (max) as shown in Figures 20 and 25, Appendix III. It then follows that if we continue to assume a power law spectrum to ranges beyond E_3 (max), then the exponent drops to $\gamma \approx 3$. Thus in the discussion which follows we shall assume a differential power law spectrum with $3 < \gamma < 5$.

We may determine the electron flux for the time interval August 7 - 14, 1959 at E_3 (max) in the equatorial plane as follows. The counting rate, I, of a single proportional counter is given by

$$I = \int_{E_1}^{E_2} N(E)\, G(E)\, dE$$

where N(E) is the electron differential energy spectrum and G(E) is the response function of our detector, shown in Figure 4. The lower limit E_1 is not critical for determining I since the function G(E) falls off faster than $E^{4.7}$ below 100 Kev. On the other hand, the value of ρ_e is extremely sensitive to E_1 since the power spectrum is divergent as $E_1 \longrightarrow 0$. For the present case we set $E_1 \approx$ 100 Kev. The upper limit, E_2, is not well known. From Walt, et al, it should be less than 800 Kev. From the results of Van Allen and the Soviet measurements, E_2 is consistent with a value less than 1000 Kev. Therefore, we assume E_2 = 1000 Kev.

The parameter A in the expression $AE^{-\gamma}$ depends very little on the choice of E_1, but is sensitive to the choice of E_2. Increasing E_2 reduces A.

The values for the integral electron flux in the region E_3 at the geomagnetic equator are given for $\gamma = 3$ and $\gamma = 5$ in Table II, along with the parameters used in the calculations. To show that the results are not very sensitive to the choice of the upper limit E_2, flux values for both $E_2 = 1$ Mev and $E_2 = 2$ Mev are given.

The electron energy density is then,

$$\rho_e = \int_{E_1}^{E_2} \frac{N(E)}{v_e(E)} E \, dE$$

where $v_e(E) = c\left[\frac{\eta(\eta+2)}{\eta+1}\right]^{\frac{1}{2}}$ is the velocity of the electrons, $\eta = E/m_e c^2$, and m_e and c are the electron mass and the velocity of light, respectively. The computed values of ρ_e are given in Table II.

Since there is some evidence (Vernov, Chudakov, Vakulov and Logachev, 1959) that there are electrons in the spectrum below 100 Kev, our calculations tend to be lower limits. We also note that the total intensity at E_3 (max) increased sixfold at the equator by August 21 still under the condition $\rho_m > \rho_e$ (with the spectrum essentially unchanged as shown in Figure 22). Thus it is clear that the exponent cannot be much in excess of $\gamma = 3$, under the assumption of a power law spectrum.

In Table III a similar analysis in the region of E_2 (max) at $R_o \approx$ 16 - 17,000 Km shows that $\rho_e \ll \rho_m$ even for the case of $\gamma = 5$.

XII. SUMMARY AND DISCUSSION

a) Structure of the outer belt, the geomagnetic field, and fluxes of electrons and protons

Measurements of bremsstrahlung in the satellite Explorer VI have revealed that for about two months there existed two distinct peaks of electron intensity, identified as regions E_2 and E_3. This kind of structure is a persistent feature of the outer belt. It is proved that the maximum intensity in the E_3 region coincides over a wide range of geomagnetic latitudes with magnetic lines of force in the centered dipole approximation. Thus, the measured electron intensity maxima may be used as tracers of the geomagnetic field lines of force for the purpose of analyzing changes in the belt with time. During geomagnetic storms the electron intensity increased many-fold at E_3 (max), but even under these conditions the trace of the intensity maximum followed a center dipole line of force. This leads to the conclusion that the electron energy density must have been everywhere less than the magnetic energy density throughout the time of our measurements.

The observed range for the maximum electron intensity undergoes large and rapid inward shifts during geomagnetic storms which amount to as much as 10% of the total range of the outer belt. This effect is likely to have its origin beyond the range of E_3 and connected with the irreversible energy gain in the outer belt discussed later in this section.

By introducing the assumption that the bremsstrahlung is produced by an electron spectrum of the form $E^{-\gamma}$, and by noting that the particle energy density is everywhere less than the magnetic energy density, we may calculate the maximum allowed electron fluxes in the region of E_3 under a variety of assumptions. For this assumed spectrum and energy limits of 100 - 1000 Kev, we find that γ should be close to 3 and cannot be as large as 5. This agrees with independent calculations derived from the measured ratio of G. M. counter to proportional counter counting rate. Under these assumptions the omnidirectional electron flux at R_o = 22,000 Km. is 8 x 10^8 electrons/cm^2 sec. At smaller range in the E_2 region, a larger value for the exponent is allowed from energy density arguments, and is calculated from the observed change in counting rates of bremsstrahlung detectors. For the region E_2 a value of $\gamma = 5$ is consistent with high latitude observations.

The bremsstrahlung detector data show that the energy spectrum along a line of force E_3 (max) is essentially independent of latitude, but through E_2 (max) is sensitive to geomagnetic latitude, being strongly energy dependent at high latitudes. For example, if the electron energy spectrum has the form $E^{-\gamma}$ with an upper energy limit between 1000 and 2000 Kev, then the form of the spectrum in the outer belt tends to become flatter (decreasing γ) with increasing range in the outer belt. The electron spectrum near E_3 (max) was observed to remain essentially unchanged

even though the intensity changed over a factor of 6 as a result of a geomagnetic storm. At a later time, the spectrum was observed to change significantly and in such a way that for our assumed spectrum the value of the exponent increased by 25 to 50% within a few days, and persisted long after the termination of the magnetic storm. Thus, it is evident that geomagnetic storms may induce changes of the outer belt electron spectrum as well as changes in total intensity.

The proton flux in the outer belt for energies in excess of 75 Mev is (0.0 ± 0.1) protons/cm^2 sec.

b) The Origin of the Outer Belt Electrons

We have described properties of the outer electron belt (in Section IX) by four parameters representing equatorial intensity $I_o(t)$, location of the magnetic dipole line of force through E_3 (max) at the equator, R_o, the electron density distribution along a line of force $I = I_o\left(\frac{B}{B_o}\right)^{-x}$ characterized by the parameter x, and a measure Z of spectral change of electrons with time. We find that within the sequences of changes in the outer belt induced by geomagnetic storms, there are some changes of these parameters which are accounted for only by invoking an irreversible energy gain or energy loss within the belt. Since we measure bremsstrahlung, our count rate I (single counter) is given by

$I = \int_0^\infty G(E)\, N(E)\, dE$, where N(E) is the spectrum and G(E) is the detector efficiency. Although we know G(E) (See Figure 4), we do not know N(E) and therefore cannot prove whether a change in I arises from the gain or loss of particles, or whether there is a kinetic energy gain or loss for a conserved number of particles. Thus, we confined our conclusions to the proof that there exist two kinds of irreversible processes; namely,

1. Particle or energy gain to the belt.
2. Particle or energy loss, leading to a stable intensity and electron mirror-point distribution.

Regarding the process of energy gain we have found arguments which strongly favor local acceleration of the electrons. Some of these arguments are of the negative kind. The monitoring of the high energy electron flux beyond the outer belt proves that preaccelerated electrons are not present with sufficient density even if it were possible to trap them efficiently. An injection of electrons at sub-detection energies (< 50 Kev) followed by local acceleration is unlikely because the electron distribution of added particles would have to maintain the original E_3 (max) location in the magnetic field and leave the resultant energy spectrum unchanged.

We are led, therefore, to consider mainly local acceleration of electrons already trapped and to ask where and at what times during the magnetic storm could this

irreversible energy gain occur. The time of occurrence is fairly well limited to the last part of the main phase and extending through the first hours of recovery from the main phase of the geomagnetic storm. (August 18 and 19 as shown in Figures 13 and 23).

The mechanism for energy gain in this period is obscure. For example, if a statistical acceleration process, like Fermi acceleration were operative at this time while small scale magnetic irregularities were moving through the dipole field we might expect that protons would be even more efficiently accelerated than electrons. Is it not likely that the sudden increase of particle intensity observed in the Explorer VI scintillator (Rosen and Farley 1961) could be the low energy protons beginning at the time when all bremsstrahlung detectors and the ion chamber still observed low intensity on August 17? The scintillator detects protons of energy $\geq$ 2 Mev. It may also be argued that the energy input is coincident with the rapid recovery of the geomagnetic field -- such as ring current changes -- on August 17-18. In any case, any successful model of acceleration must include, 1) the preservation of E_3 (max) over an intensity range of factor six, 2) no drastic changes in the form of the spectrum, and 3) a concentration of the excess intensity in the vicinity of the equator.

The loss processes are of a different kind. They are associated with a changing spectrum, a decrease of electron pitch angles and a gradual reduction of intensity.

All these changes occur while the geomagnetic field gradually increases to its prestorm level and becomes unperturbed. The loss process seems to go on with a longer time constant than the irreversible acceleration discussed above. Again we are not sure whether particles are escaping from the trapped distribution or whether we are observing particle deceleration. The changes are consistent with the latter alternative, especially if we assume a spectrum of the form $E^{-\gamma}$. We then interpret the losses of particles or energy in two successive stages: first, there is a loss at high pitch angles and high energy, and second, there is a loss at all latitudes independent of pitch angle.

The changes take place as though there existed some instability, or energy loss process (possibly radiative) which returns the electron intensity distribution to the "steady state". In fact, one of the most remarkable results of our analysis is the observed tendency for the E3 region to stabilize around a characteristic pitch angle distribution where $x \approx 0.6$ except during magnetic field perturbations. Note that $x \approx 0.6$ even for the period after the September 3 magnetic storm (Fig. 16).

The fluctuations of high energy electron intensity beyond the outer belt introduce the possibility that there may also be a loss of particles in near-equatorial orbits on or about August 20 when the equatorial concentration of electrons was greatest.

It has been suggested (Arnoldy, Hoffman and Winckler, 1960b; O'Brien, Van Allen, Roach and Gartlein, 1960) that the large reduction in observed bremsstrahlung intensity with the main phase of a magnetic storm (in our case pass 19) is in reality "dumping" of particles to form the aurora. We believe that the small energy density of high energy electrons cannot account for the much larger auroral energy release and that betatron deceleration between t_1 and t_2 is more likely.

The results are consistent with the acceleration of ambient electrons to the observed energy distributions. Probably through collective motions of high temperature solar plasma somewhat more energetic particles could be trapped from time to time, but their equilibrium energies and distribution would still be dominated by processes in the geomagnetic field. In view of our conclusions, the question of the origin of energy gain and loss processes is more significant than the question: from where do the electrons come?

The beta-decay electrons from neutrons certainly contribute to the outer belt (Hess, 1960; Dessler and Karplus, 1960). Recently, however, it was shown that processes other than injection of neutron decay electrons must be operative in order to account for the spatial distribution of electrons in the outer belt (Hess, Killeen, Fan, Meyer and Simpson, 1961). This again points to the existence of energy gain and loss processes.

It is important to note that satellite bremsstrahlung observations in low altitude orbits, such as Explorer VII, will appear to have a time dependence different from our equatorial results for the outer belt. This is readily understood from Figures 14 and 23 for the August 1959 magnetic storms. For example, the increase of intensity would appear at the "tip" of the outer belt a few days after reaching maximum intensity at the equator. The position in latitude of the maximum intensity near the "tip" should shift rapidly by $\sim$ 1° to 3° corresponding in our analysis of changes in R_o (note that for low altitudes the center dipole approximation is not sufficient to describe the real field).

Finally, we caution the reader to recall that we have been able to analyze only two magnetic storms. We would expect the detailed changes in the outer electron belt from one magnetic storm to another to be as diverse as geomagnetic storms themselves have proven to be through many years of analysis by many investigators. Indeed, the magnetic storm of September 3 (for which we have very few data) did not lead to an irreversible acceleration, but only a loss mechanism which preserved the prevailing electron pitch angle distribution.

ACKNOWLEDGMENTS

It is a pleasure to acknowledge the essential contribution to the engineering of our apparatus in Explorer VI by L. Petraitis, R. Takaki, J. Jewzeski and J. Lamport of the Universities' Laboratories for Applied Sciences. For data reduction and analysis we thank C. Gloeckler, M. Case, K. Schwarz and G. Lentz. A continuous watch for unusual solar events by R. Tjonaman and the staff of the Cosmic Ray Group assisted in increasing the data acquisition during August 1959. The assistance of R. D'Arcy in the X-ray calibration of the duplicate payload was appreciated. We thank R. S. Rochlin and the General Electric Co. for the use of their linear accelerator and D. Yovanovitch for assistance in carrying out the proton calibrations.

Discussions of our results with E. N. Parker have been both stimulating and helpful to us.

We appreciate the collaboration among those conducting experiments in Explorer VI, especially the Minnesota group of Arnoldy, Hoffman and Winckler and the Space Technology group of A. Rosen, T. Farley and E. Smith where we have mutually exchanged data. We thank the Minnesota group for permission to use their unpublished G. M. counter data and the use of their X-ray apparatus.

In carrying out the Explorer VI project we are especially indebted to J. Lindsay and H. Newell of the National Aeronautics and Space Administration, and A. Thiel, J. Lindner and K. Moe of Space Technology Laboratories.

List of Tables

Figure Captions

Figure 1. Perspective drawing of the Explorer VI satellite orbit. The orbital data are as follows:

Period: 12 hours 48 minutes

Apogee: 48,788 Km.

Perigee: 6,626 Km.

Geographic inclination: 47°

Tilt of orbit: 38° with respect to ecliptic plane.

Figure 2. Block diagram of instrumentation in Explorer VI used for the analysis of the outer electron belt.

Figure 3. Detector response for protons from the synchro-cyclotron beam of the University of Chicago.

Figure 4. Calibration curve for the center counter shown in Figure 2. These electron data were obtained with the detector in the duplicate Explorer VI vehicle.

Figure 5. Counting rate data along the satellite trajectory (Pass No. 27) showing the existence of the high energy proton region P_1 (inner belt) and the E_3 peak from electrons in the outer belt. Note that the triple coincidence (proton) count rate beyond P_1 is due to cosmic radiation alone.

Figure 6. Counting rate data along the satellite trajectory (Pass No. 13) showing the existence of regions P_1 (inner belt), E_2 and E_3 (outer belt). Statistical errors are approximately the size of individual data points.

Figures 7a and 7b. Counting rate from bremsstrahlung as a function of range along the satellite trajectory. Electron peaks E_1 and E_2 are shown. All the data points which determine the curves for each pass are shown here. Statistical errors are less than $\pm$ 1%.

Figure 8. Proof that the outer belt maximum E_3 (max) lies on magnetic lines of force in the centered dipole approximation even for periods of geomagnetic storms.

Figure 9. Projection of satellite orbit on the meridian plane of the geomagnetic field using the centered dipole approximation. Insert (b) shows the complete trajectory.

Figure 10. Representation of Explorer VI trajectory in coordinates R_o vs. R in the approximation of a centered dipole magnetic field where $R = R_o \cos^2 \lambda$.

Figure 11. Meridian plane plot of the E_2 (max) and E_3 (max) positions in the geomagnetic field. For more detailed analysis see Figures 8 and 23.

Figure 12. The position of E_3 (max) extrapolated to the geomagnetic equatorial range R_o as a function of time.

Figure 13a. The change of intensity of E_3 (max) in the geomagnetic equator ($\pm$ 10°) as a function of time. The averaged values of the surface horizontal component of the equatorial geomagnetic field (Huancayo, Peru) is shown. The A_p index indicating the magnitude of geomagnetic fluctuations is given as individual solid points.

Figure 13b. Changes in magnetic field intensity observed in Explorer VI within the outer belt (Smith and Rosen, 1960; Smith and Sonett, 1961 to be published).

Figure 14. Electron intensity as a function of time at E_3 (max) for different geomagnetic latitude intervals. The solid points represent data within $\pm$ 5° of the 20° curve or the 40° curve.

Figure 15. Electron intensity at E_3 (max) along lines of force in the centered dipole approximation.

Figure 16. All experimental data for E_3 (max) along lines of force similar to Figure 15, but covering a wide interval of time and range in space.

Figure 17. Electron intensity along magnetic lines of force through E_3 (max) as a function of time. Using the data from Figure 15 and data during the geomagnetic storms August 16 - 20, it is shown that $I = I_o\left[\frac{B}{B_o}\right]^{-x}$.

Figure 18. Electron intensity along magnetic lines of force through E_3 (max) as a function of time later than August 26, 1959.

Figure 19. For the region of E_2 (max) the intensity along lines of force have been determined by using data in the following time intervals:

A_2 : August 7 to 15, 1959.

B_2 : August 17 to 18.

C_2 : September 8 to 11.

D_2 : September 24 to 25.

Figure 20. The ratio Z of counting rates from two bremsstrahlung detectors as a function of equatorial range R_o. All data points have been projected onto equatorial plane in the centered dipole magnetic field approximation. A change in Z indicates a change in electron spectrum. (The G. M. counter data are from Arnoldy, Hoffman and Winckler, 1960a, b and private communications).

Figure 21. The ratio Z along magnetic lines of force near E_3 (maximum) and E_2 (maximum).

Figure 22. The ratio Z as a function of the single proportional counter counting rate at E_3 (max).

Figure 23. The changes in pitch-angle (or mirror point) distributions and intensity for electrons at E_3 (max) as a function of range R_o, and time for the geomagnetic storms of August 16 and 20, 1959.

Figure 24. The high energy electron flux observed beyond the outer electron belt, i.e. at a range $R_o \geq$ 40,000 Km. as a function of time.

Figure 25. The calculated relationship between the ratio Z and the exponent γ, assuming that the electron spectrum is $dN = AE^{-\gamma} dE$ ($E \leq$ 1 Mev.).

Table I

Values of Exponent x as a Function of Time at Intermediate Latitudes

Pass (Day)	x	$R/\cos^2\lambda$
Curve A (8-18 to 8-19)	0.98	23480
22 (8-18)	0.91	21480
23 (8-19)	0.93	23400
28 (8-21)	0.79	20820
Curve B (8-26)	0.83	20900
43 (8-29)	0.80	20790

Table II

Parameters for Electron Flux and Energy Density in Region E_3 at the Geomagnetic Equator

γ	E_1 Kev	E_2 Kev	A $\frac{\text{electrons}}{\text{cm}^2\ \text{sec}}$ (Kev)$^{\gamma-1}$	N(E > 100Kev) electrons/cm^{2}sec	ρ_e ergs/cm^3	ρ_m ergs/cm^3
3	100	1000	1.6×10^{13}	8×10^8	4×10^{-8}	2×10^{-6}
3	100	2000	2.4×10^{12}	1.2×10^8	6.8×10^{-9}	
5	100	1000	5×10^{18}	1×10^{10}	8×10^{-7}	2×10^{-6}
5	100	2000	2.8×10^{18}	7×10^9	3.3×10^{-7}	
Equilibrium Spectrum from Neutron Decay Only*	0	800	5.3×10^{-5}	N(E ≥ 0 Key) 4.4×10^8	3.6×10^{-8}	2×10^{-6}

* Based on spectrum from Hess and Poirier (Private Communication to J.A.S.)

Table III

Parameters for Electron Flux and Energy Density in Region E_2

γ	E_1 Kev	E_2 Kev	A $\frac{\text{electrons}}{\text{cm}^2 \text{ sec}}$ (kev)$^{\gamma-1}$	N(E > 100 Key) electrons/cm^{2}sec	ρ_e ergs/cm^3	ρ_m ergs/cm^3
3	100	1000	1.1×10^{13}	5.3×10^{8}	2.9×10^{-8}	1×10^{-5}
3	100	2000	1.6×10^{12}	8×10^{-9}	4.4×10^{-9}	
5	100	1000	3.3×10^{18}	7×10^{9}	5.2×10^{-7}	1×10^{-5}
5	100	2000	1.9×10^{18}	4.7×10^{9}	2.2×10^{-7}	

References

ARNOLDY, R., R. HOFFMAN AND J. R. WINCKLER, "Measurements of the Van Allen Radiation Belts During Geomagnetic Storms", pp. 877-896 of "Space Research" ("Proceedings of the First International Space Science Symposium"), edited by H. Kallman Bijl, No. Holland Publishing Co.,1195 pp., Amsterdam, 1960a.

ARNOLDY, R. L., R. A. HOFFMAN AND J. R. WINCKLER, "Observations of the Van Allen Radiation Regions during August and September 1959. Part 1". J. Geophys. Res., 65, 1361-1375, 1960b.

CLADIS, J. B., L. F. CHASE, W. L. IMHOF AND D. J. KNECHT, "Energy spectrum and angular distributions of electrons trapped in the geomagnetic field." Technical Report LMSD-895085 (1961).

DESSLER, A. J. AND R. KARPLUS, "The Gap in the Electron Component of the Outer Zone of the Van Allen Radiation," J. Geophys. Research, 65, 2486, 1960.

FAN, C. Y., P. MEYER AND J. A. SIMPSON, "Trapped and Cosmic Radiation Measurements from Explorer VI," pp. 951-966 of "Space Research."
(Proceedings of the First International Space Science Symposium) Edited by H. Kallman Bijl, North Holland Publishing Co., 1195 pp, Amsterdam, 1960.

FAN, C. Y., P. MEYER, AND J. A. SIMPSON, "Equatorial Pitch Angle Distributions of Electrons in the Outer Radiation Belt,"Proceedings of the second International Space Science Symposium - Florence, Italy, April, 1961.

FARLEY, T. A. and A. ROSEN, "Charged Particle Variations in the Outer Van Allen Zone During a Geomagnetic Storm," J. Geophys. Res. 65, 3494 (1960).

FREDEN, S. C. and R. S. WHITE, "Particle Fluxes in the Inner Radiation Belt," J. Geophys. Res., 65, 1377-1383, 1960.

GOLD, T., "Motions in the Magnetosphere of the Earth," J. Geophys. Res., 64, 1219-1224, 1959.

HERLAFSON, N., "Diffusion of Particles in the Earth's Radiation Belts," Phys. Rev. Letters, 5, 414 (1960).

HESS, W. N., "The Radiation Belt Produced by Neutrons Leaking out of the Atmosphere of the Earth," J. Geophys. Res. 65, 3107-3115 (1960).

HESS, W.N., J. KILLEEN, C. Y. FAN, P. MEYER and J. A. SIMPSON, "The Observed Outer Belt Electron Distribution and the Neutron Decay Hypothesis," J. Geophys. Res. (in publication, 1961).

NORTHROP, T. G., and E. TELLER, "Stability of the Adiabatic Motion of Charged Particles in the Earth's Field," Phys. Rev. 117, 215-225, 1960.

O'BRIEN, B. J., J. A. VAN ALLEN, F. E. ROACH, and C. W. GARTLEIN, "Correlation of an Auroral Arc and a Subvisible Monochromatic 6300 A Arc with Outer-zone Radiation on November 28, 1959," J. Geophys. Res. 65, 2759-2766, 1960.

PARKER, E. N., "Effect of Hydromagnetic Waves in a Dipole Field on the Longitudinal Invariant," J. Geophys. Res. 66, 693-708 (1961a).

PARKER, E. N., "The Distribution of Trapped Particles in a Changing Magnetic Field," J. Geophys. Res., to be submitted, (1961b).

POST, R. F., AND W. A. PERKINS, Phys. Rev. Let. 5, 85 (1961) (and private communication to J.A.S.)

ROSEN, A., T. A. FARLEY and C. P. SONETT, "Soft Radiation Measurements on Explorer VI Earth Satellite," pp. 938-950 of "Space Research"("Proceedings of the First International Space Science Symposium"), edited by H. Kallman Bijl, North Holland Publishing Co., 1195 pp., Amsterdam, 1960.

ROSEN, A. AND T. A. FARLEY, "Characteristics of the Van Allen Radiation Zones as Measured by the Scintillation Counter on Explorer VI," J. Geophys. Research (to be published) 1961.

SMITH, E. AND ROSEN, A , "The Scientific Results of the Satellite: Explorer VI," p. 405 of "Ballistic Missile and Space Technology," edited by D. P. LeGalley, Acad. Press, 1960.

SMITH, E. AND C. P. SONETT, "Scientific Observation of a Ring Current during Magnetic Storm: Explorer VI." J. Geophys. Res., to be submitted (1961).

SONETT, C. P., E. J. SMITH, D. L. JUDGE AND P. J. COLEMAN, JR., "Current Systems in the Vestigal Geomagnetic Field: Explorer VI," Phys. Rev. Letters, 4, 161-163, 1960.

VAN ALLEN, J. A., C. E. MC ILWAIN AND G. H. LUDWIG, "Radiation Observations with Satellite 1958 Epsilon," J. Geophys. Research, 64, 271-286, 1959a.

VAN ALLEN, J. A., C. E. MC ILWAIN AND G. H. LUDWIG, "Satellite Observations of Electrons Artificially Injected into the Geomagnetic Field," J. Geophys. Research, 64, 877-891, 1959b.

VERNOV, S. N., A. YE. CHUDAKOV, P. V. VAKULOV, AND YU. I. LOGACHEV, "Study of Terrestrial Corpuscular Radiation and Cosmic Rays by the Flight of a Cosmic Rocket," Doklady Akademii Nauk SSSR 125, 304-307, 1959.

VERNOV, S. N. AND CHUDAKOV, A. E., "Terrestrial Corpuscular Radiation and Cosmic Rays," pp. 751-796 of "Space Research." (Proceedings of the First International Space Science Symposium), edited by H. Kallman Bijl, North Holland Publishing Company, 1195 pp., Amsterdam, 1960.

WALT, M., L. F. CHASE, JR., J. B. CLADIS, W. L. IMHOF AND D. J. KNECHT, "Energy Spectra and Altitude Dependence of Electrons Trapped in the Earth's Magnetic Field," pp. 910-920 of "Space Research" (Proceedings of the First

International Space Science Symposium), edited by H. Kallman Bijl, North Holland Publishing Company, 1195 pp., Amsterdam, 1960.

Appendix I
Table I

Characteristics of Charged Particle Detectors and Magnetometer on Explorer VI

Proportional Counter Telescope	University of Chicago
a) Triple coincidence counts measure protons ($E > 75$ Mev) and electrons ($E > 13$ Mev) and are not affected by intense bremsstrahlung.	
b) Single counts measure bremsstrahlung and particles under a)	
G. M. Counter and Ion Chamber	University of Minnesota
a) G.M. counter measures sum of protons ($E > 36$ Mev) Electrons ($E > 2.8$ Mev) and ambient bremsstrahlung	
Ion Chamber b)/measures average ionization per particle (Protons $E > 24$ Mev, Electrons $E > 1.6$ Mev) plus bremsstrahlung	
Plastic Scintillation Counter	Space Technology Laboratories
a) Measures electron flux directly for $E > 200$ Kev.	
plus b) Bremsstrahlung	
plus c) Protons with $E > 2$ Mev.	
Spin Magnetometer	Space Technology Laboratories
Measures component of magnetic field perpendicular to the spin axis of Explorer VI down to 10^{-4} gauss.	

Appendix I
Table II

Low Latitude Traversals Through the Outer Radiation Belt Which Yielded Data

		Dates	Number of Passes through outer belt.
1.	Pioneer I		1
2.	Pioneer III		1
3.	Lunik I	Jan.2,1959	1
4.	Pioneer IV		2
5.	Explorer VI	Aug.7-Oct.6, 1959	113
6.	Lunik II	Sept.12, 1959	1
7.	Pioneer V	Mar.11, 1960	1

Appendix I
Table III

TIMES FOR ORBIT PASS NUMBERS OF EXPLORER VI(Aug.7-Oct.6,1959)

Date	Pass No.	Date	Pass No.	Date	Pass No.
8-7	1	8-28	41	9-19	81
8	2	29	42	19	82
8	3	29	43	20	83
9	4	30	44	20	84
9	5	30	45	21	85
10	6	8-31	46	21	86
10	7	9- 1	47	22	87
11	8	1	48	22	88
11	9	2	49	23	89
12	10	2	50	23	90
12	11	3	51	24	91
13	12	3	[illegible]	24	92
13	13	4	[illegible]	25	93
14	14	4	[illegible]	25	94
15	15	5	[illegible]	26	95
15	16	5	[illegible]	26	96
16	17	6	57	27	97
16	18	6	58	28	98
17	19	7	59	28	99
17	20	7	60	29	100
18	21	8	61	29	101
18	22	8	62	30	102
19	23	9	63	9-30	103
19	24	10	64	10- 1	104
20	25	10	65	1	105
20	26	11	66	2	106
21	27	11	67	2	107
21	28	12	68	3	108
22	29	12	69	3	109
23	30	13	70	4	110
23	31	13	71	4	111
24	32	14	72	5	112
24	33	14	73	5	113
25	34	15	74		
25	35	15	75		
26	36	16	76		
26	37	16	77		
27	38	17	78		
27	39	17	79		
28	40	18	80		

Appendix II

The Process of Determining the Position of a Radiation Belt

We define the position of a radiation belt by the location in the geomagnetic equatorial surface at which the counting rate of a radiation detector is a maximum.

Consider a line of force of the geomagnetic field. A position on this line may be specified by means of a parameter $b = B/B_o$ where B is the magnetic field intensity at this position, while B_o is the minimum magnetic field intensity along the line of force. Since an equatorial surface is a surface generated by the points of minimum field intensity on lines of force, i.e. the B_o surface, the constant B_o lines and their orthogonal lines, denoted by constant ϕ, may then be conveniently used as a coordinate system to specify the positions of lines of force. Thus, the three variables, B_o, ϕ and b determine a point in space, and we can write the counting rate as

$$I = I(B_o, \phi, b). \tag{1}$$

The variation of counting rate per unit arc length ds along the trajectory of the satellite is

$$\frac{dI}{ds} = \left[\frac{\partial I}{\partial B_o}\right]_{\phi,b} \frac{dB_o}{ds} + \left[\frac{\partial I}{\partial \phi}\right]_{B_o,b} \frac{d\phi}{ds} + \left[\frac{\partial I}{\partial b}\right]_{B_o,\phi} \frac{db}{ds} \tag{2}$$

If there is an axial symmetry so that $\left(\frac{\partial I}{\partial \phi}\right)_{B_o,\, b} = 0$, Eq. (2) becomes

$$\frac{dI}{ds} = \left[\frac{\partial I}{\partial B_o}\right]_{\phi,b} \frac{dB_o}{ds} + \left[\frac{\partial I}{\partial b}\right]_{B_o,\phi} \frac{db}{ds} \tag{3}$$

The physical meanings of $\left[\frac{\partial I}{\partial b}\right]_{B_o,\,\phi}$ and $\left[\frac{\partial I}{\partial B_o}\right]_{\phi,b}$ are respectively the variation of the counting rate along a line of force and that along the intersection of a constant b and a constant ϕ surface. The positions of the maxima shown in Fig. 5, 6, 7a, 7b are the solutions of $\frac{dI}{ds} = 0$ and are called the observed maxima whereas the true maximum of the radiation belt by our definition is given by the equation $\left[\frac{\partial I}{\partial B_o}\right]_{\phi,b} = 0$. This is, of course, correct only if the pitch angle distribution, $n(v,\theta_o)$ (Fan, Meyer, and Simpson 1961) does not vary greatly with respect to B_o.

The following is a working process by which the solution of $\left(\frac{\partial I}{\partial B_o}\right)_{\phi,b} = 0$ may be found.

It was shown in Figure 17 that for a limited segment along a line of force of a center dipole field, Eq. (1) assumes the following simple expression

$$I = f(R_o)\ (b)^{-x} \qquad (4)$$

where, if R and λ are respectively the range and the magnetic latitude,

$$R_o = R/\cos^2\lambda \quad , \quad b = \frac{(1+3\sin^2\lambda\ )^{\frac{1}{2}}}{\cos^6\lambda} \qquad (5)$$

and x is in general a function of B_o. B_o is then M/R_o^3. Therefore, if the magnetic field in the vicinity of the short portion of the trajectory is not greatly different from a center dipole field, and if the value of x is almost constant, the position of the maximum of $f(R_o)$ $(=Ib^x)$ will be approximately the solution of $\left(\frac{\partial I}{\partial B_o}\right)_{\phi,b} = 0$.

In the determination of the maximum of $f(R_o)$ we encountered two difficulties:

(1) The determination of the position of E_3 required a knowledge of the value of x for $R_o \approx 22{,}000$ Km, which is not always available. (2) The position data errors are determined by the accuracy of the trajectory data discussed below.

The values of x during the quiet period of August 7 - August 14, 1959 at $R_o = 22{,}000$ Km were 0.5 to 0.6, while in the magnetically disturbed days (August 16 - August 20) they increased to about 1.0 - 1.2. This is about the total range in the measured values of x. The following criterion was used for the actual determination. If the value of x for certain passages at R_o between 19,000 Km - 24,000 Km was available, this value was used; otherwise, the value of x of the passages immediately preceding or following was used, provided that no magnetic storms were under way.

Take the passage #20 as an example. The maximum counting rate along the trajectory ($\frac{dI}{ds} = 0$) is at $\lambda = 12.4^\circ$ and $R_o = 24{,}500$ km whereas the solution of $\frac{df}{dR_o} = 0$ is at $\lambda = 14.4^\circ$ and $R_o = 23{,}600$ km.

We have used improved trajectory calculations prepared by the staff at Space Technology Laboratories which take into account the variable atmospheric drag at perigee. These data appear to be accurate within $\approx \pm 100$ Km at the outer belt until at least September 12. However, a new

trajectory for Explorer VI will be prepared which is based on minitrack data providing more accurate position-time data at small range. In view of these trajectory errors the corrected positions of E_2 and E_3 have been worked out only for the cases where the solutions of $\frac{dI}{ds} = 0$ and $\frac{df}{dR_o} = 0$ are widely different. No corrections are needed for values of $\lambda \leq 10^\circ$, since $\frac{B}{B_o} \approx 1$.

Two final remarks must be added:

(1) Since

$$\frac{d}{ds}\left[I\left(\frac{B}{B_o}\right)^x \right] = \frac{df}{dR_o}\,\frac{dR_o}{ds}$$

there always exists an extreme value of $I\left(\frac{B}{B_o}\right)^x$ at the position where $\frac{dR_o}{ds} = 0$, and this is in general different from the solution of $\frac{df}{dR_o} = 0$.

(2) It can be shown readily that the "ridge" of equal counting-rate contours, which is frequently used as the definition of the position of a radiation belt, coincides with a line of force passing through the solution of $\frac{df}{dR_o} = 0$. Therefore, these two definitions are equivalent.

Appendix III

Derivation of Changes in Electron Spectrum Using Bremsstrahlung Detectors

We showed in Section VIII that whatever may be the form of the electron spectrum in the outer belt the spectrum undergoes changes with range and along lines of force in the vicinity of the E_2 region. However, the spectrum was approximately constant along lines of force through E_3 (max).

We shall now introduce an assumed form for the spectrum and calculate what the changes in the ratio Z of count rates from two bremsstrahlung detectors, each having different responses to a given energy spectrum. The response curve for the single proportional counter has been described in Section II and Figure 4. The response curve of the G.M. Counter in Explorer VI has been made available to us by Arnoldy, Hoffman and Winckler. (The three groups of investigators using Explorer VI for radiation measurements have exchanged their calibration and detector characteristics.)

From Section XI it appears that a reasonable form of the electron energy spectrum prevailing in the outer belt is $dN(E) = A\, E^{-\gamma}\, dE$, which we shall use in our calculations. Our second assumption is that the maximum energy for the outer belt electrons is $E < 2.8$ Mev, i.e. no direct electron detection is possible by either detector. (Arnoldy, Hoffman and Winckler, Private Communication)

We may then calculate directly the expected values of γ for given values of the ratio Z. The solid curve shown in Figure 25 uses the measured response curve in Figure 4 and a maximum electron kinetic energy of 1000 Kev. To demonstrate the sensitivity of these calculations to the shape of the response curve we have also calculated Z vs. γ for the case where the single counter response is proportional to $E^{4.7}$ over the entire energy range. Clearly, the changes in γ are not extremely sensitive to the shape of the low energy portion of the calibration curve except for high values of Z.

Thus the changes in spectrum at E_3 (max) which occur during recovery from geomagnetic storms in Figure 22 would be interpreted as a change from approximately E^{-3} to $\sim E^{-4}$ for the electron differential spectrum between August 20 and August 26, 1959.

If these assumptions were approximately correct, the dependence of Z on R_0 in Figure 20 would imply that the electron energy spectrum becomes "flatter" with increasing range.

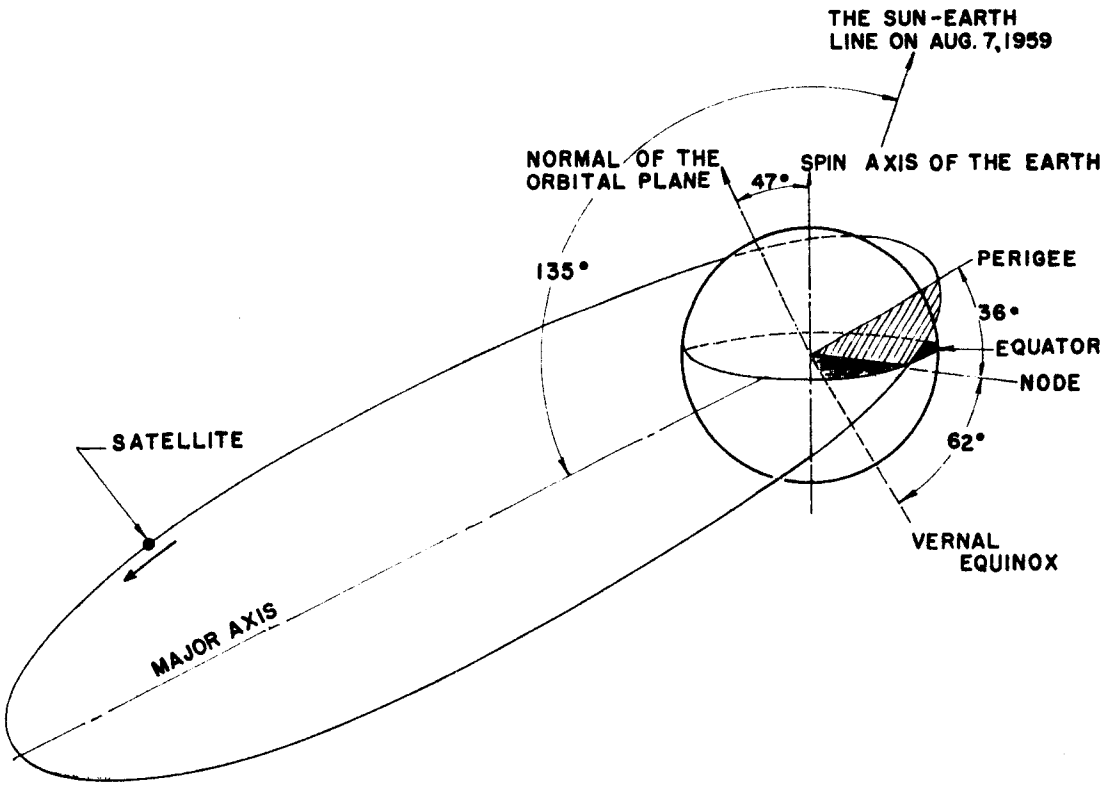
THE SUN-EARTH
LINE ON AUG. 7, 1959
NORMAL OF THE
ORBITAL PLANE
47°
SPIN AXIS OF THE EARTH
135°
PERIGEE
36°
EQUATOR
NODE
62°
SATELLITE
MAJOR AXIS
VERNAL
EQUINOX

Figure 1

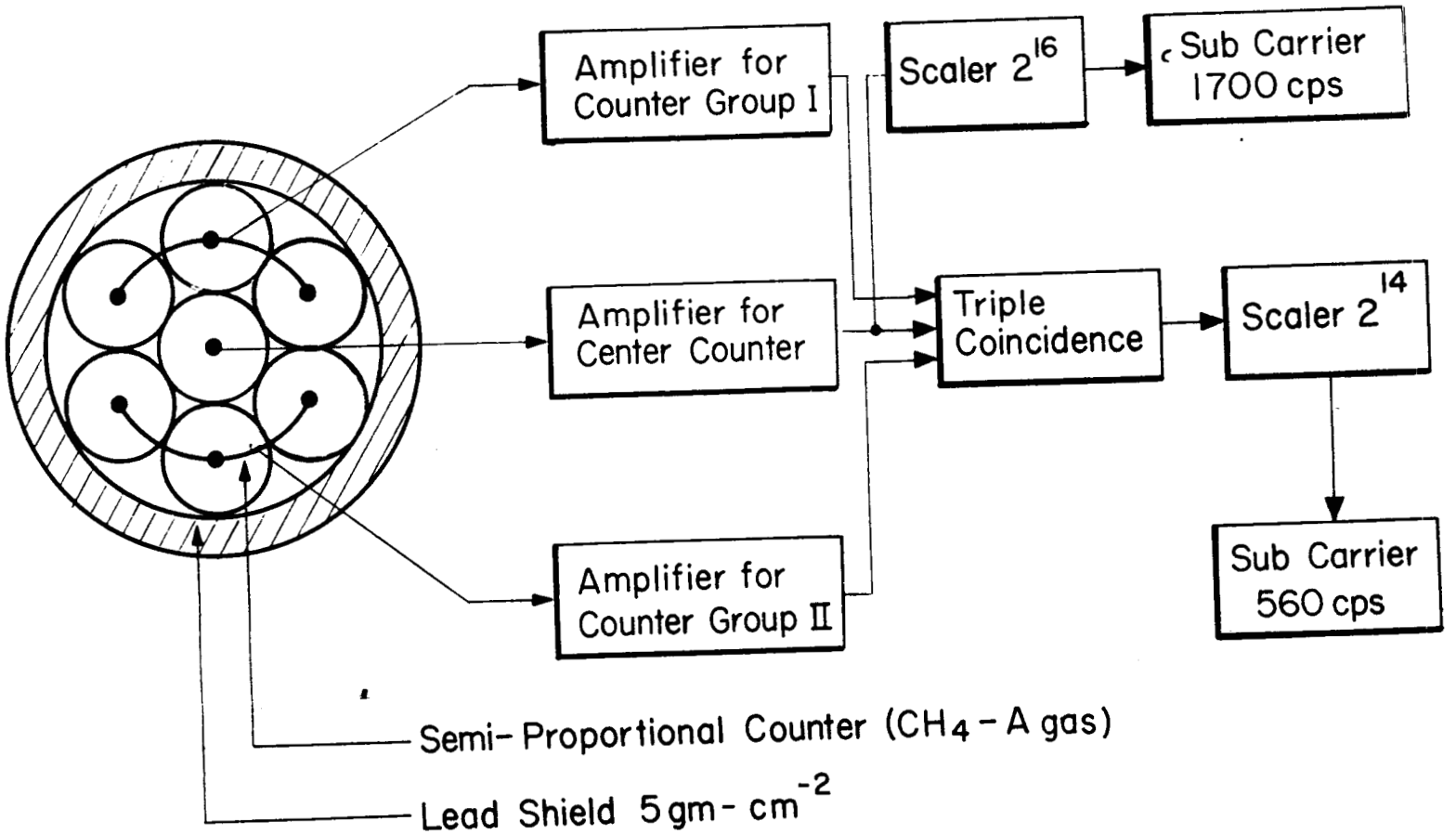

High Energy Charged Particle Instrumentation
For Explorer VI Satellite, Aug. 7, 1959

Figure 2

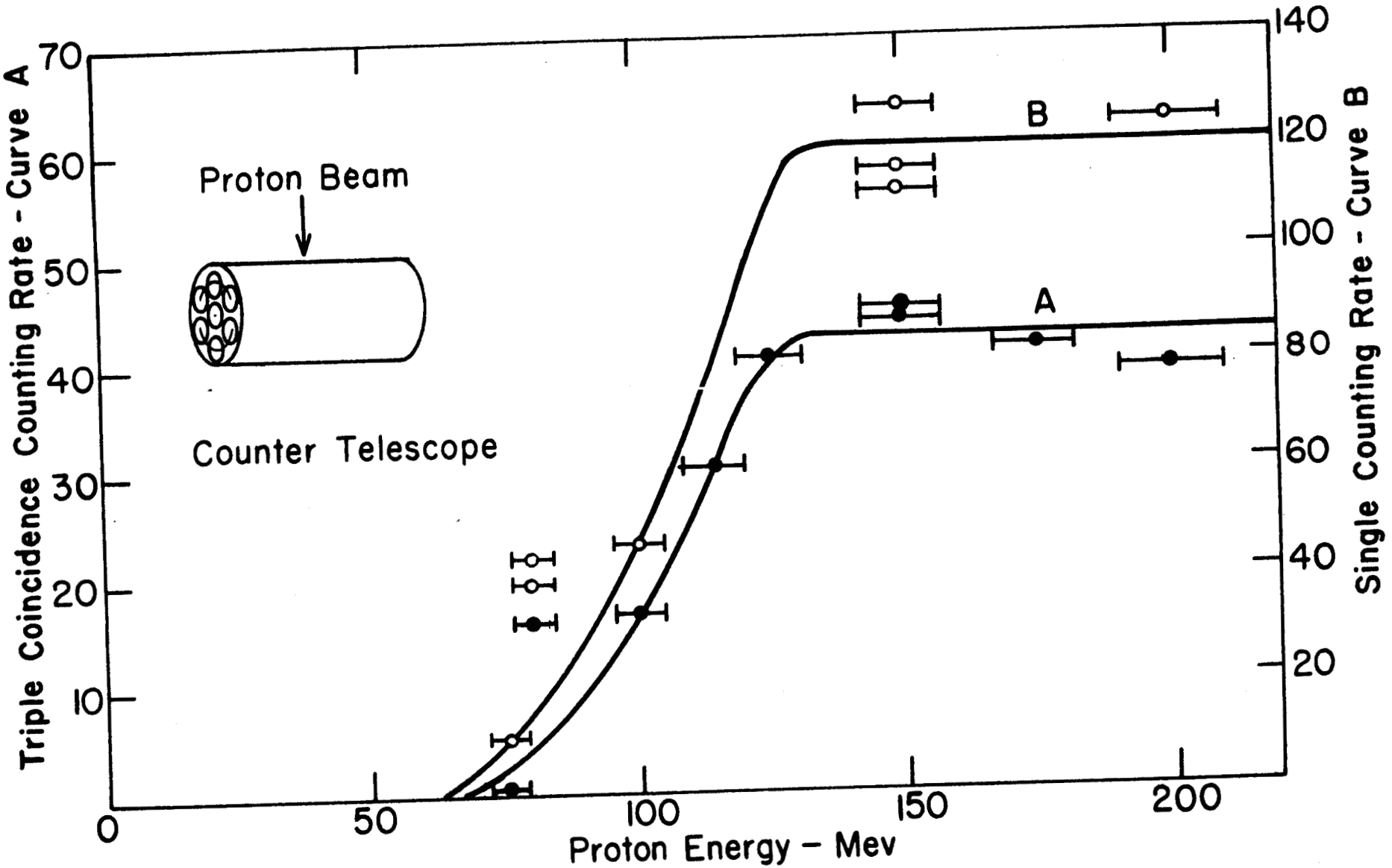
Triple Coincidence Counting Rate - Curve A
Single Counting Rate - Curve B
Proton Energy – Mev
Proton Beam
Counter Telescope
A
B
0
50
100
150
200
10
20
30
40
50
60
70
20
40
60
80
100
120
140

Figure 3

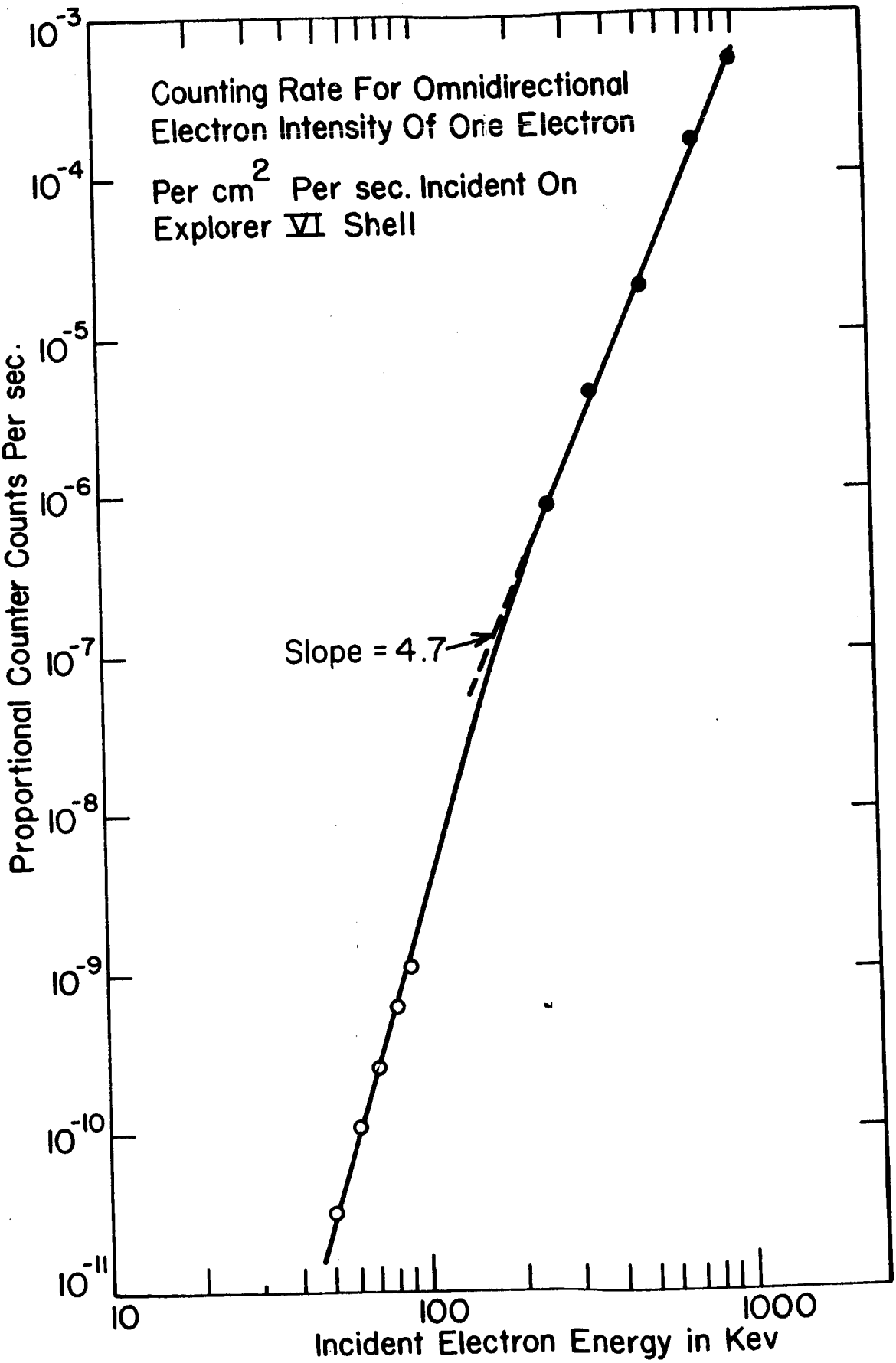
Counting Rate For Omnidirectional
Electron Intensity Of One Electron
Per cm^2 Per sec. Incident On
Explorer VI Shell
Slope = 4.7
Proportional Counter Counts Per sec.
10^{-3}
10^{-4}
10^{-5}
10^{-6}
10^{-7}
10^{-8}
10^{-9}
10^{-10}
10^{-11}
10
100
1000
Incident Electron Energy in Kev

Figure 4

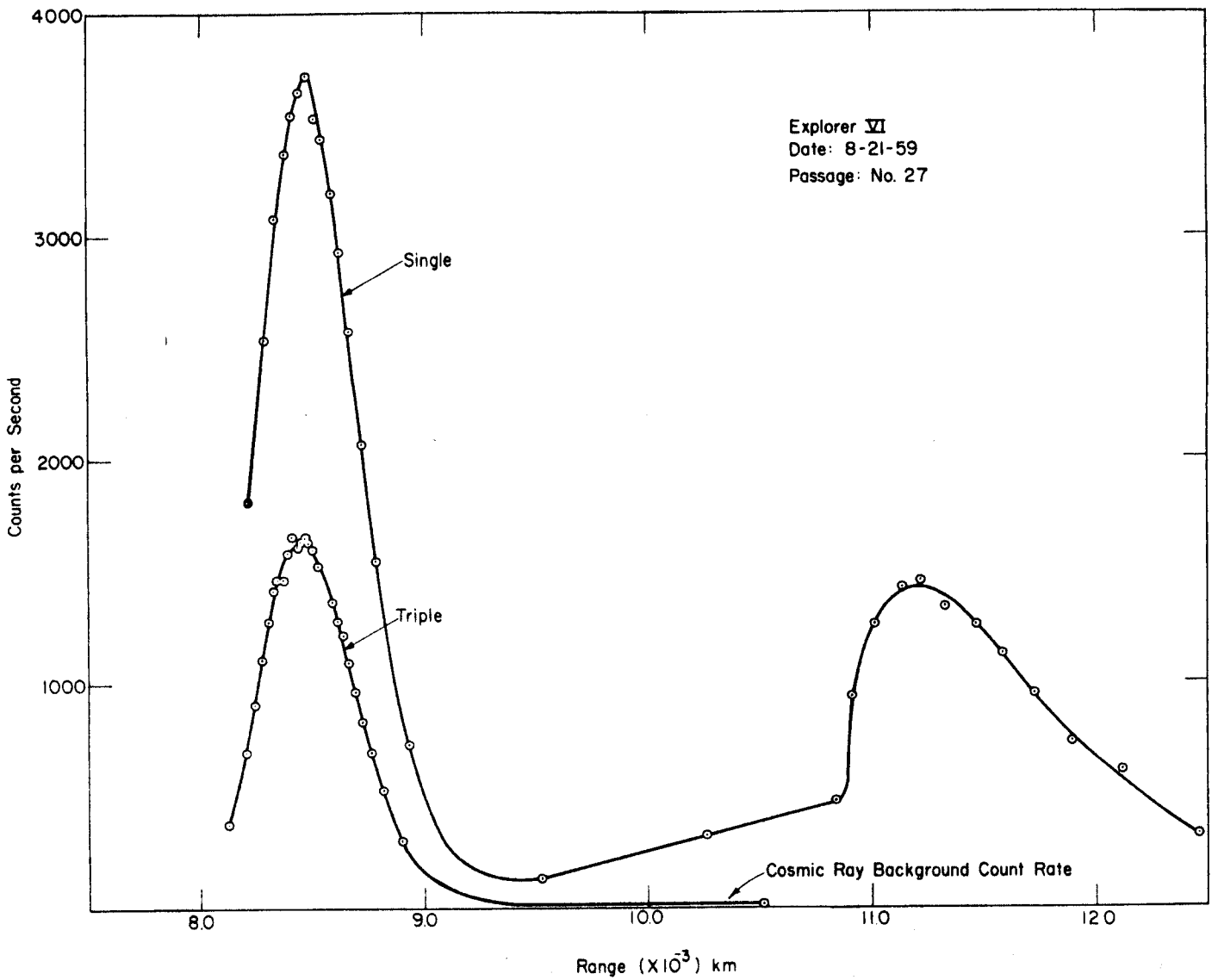
4000
3000
2000
1000
Counts per Second
Explorer VI
Date: 8-21-59
Passage: No. 27
Single
Triple
Cosmic Ray Background Count Rate
8.0
9.0
10.0
11.0
12.0
Range (X10⁻³) km

Figure 5

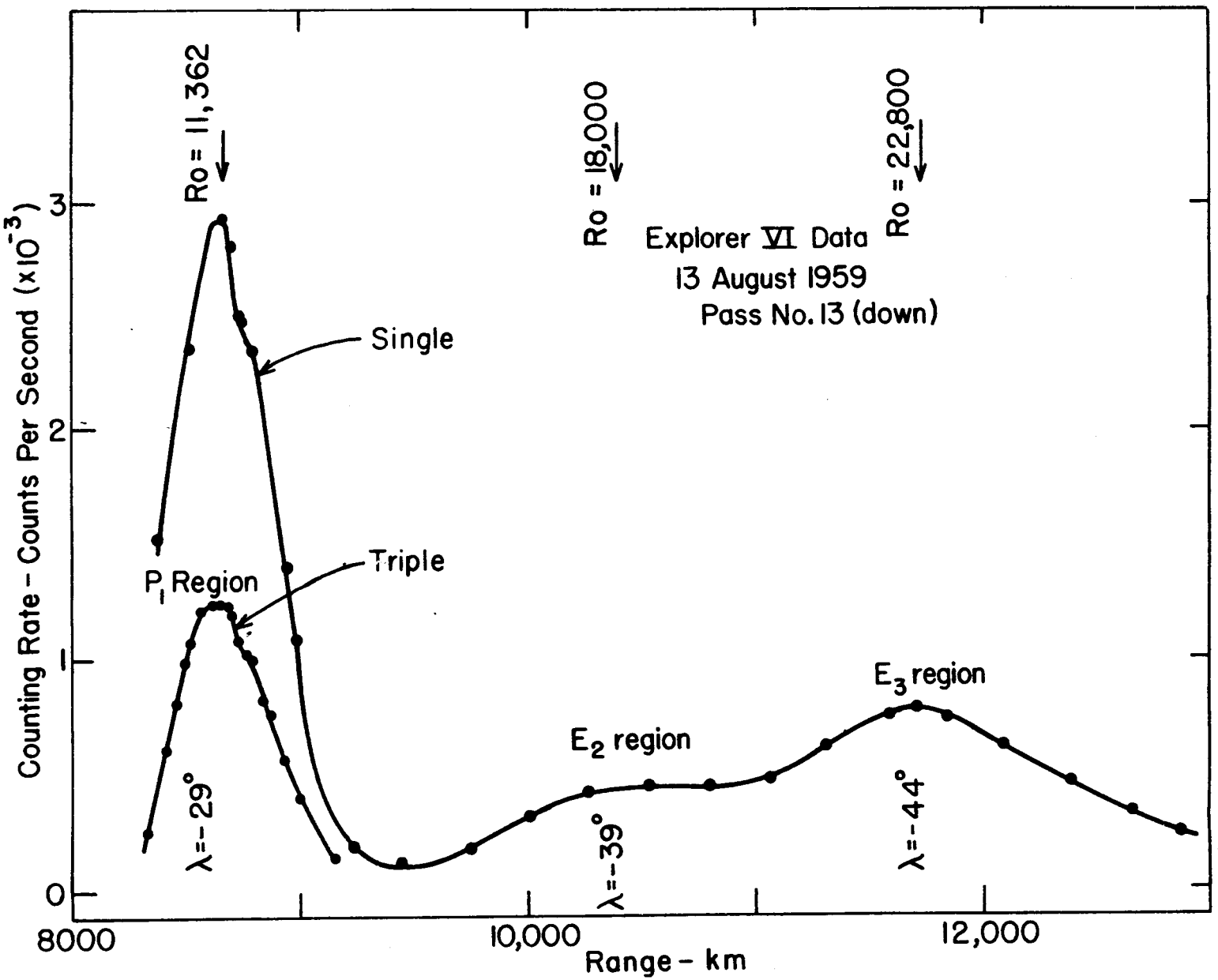
Ro = 11,362
Ro = 18,000
Ro = 22,800
Explorer VI Data
13 August 1959
Pass No. 13 (down)
Single
Triple
P1 Region
E2 region
E3 region
λ=-29°
λ=-39°
λ=-44°
Counting Rate - Counts Per Second (x10-3)
0
1
2
3
8000
10,000
12,000
Range - km

Figure 6

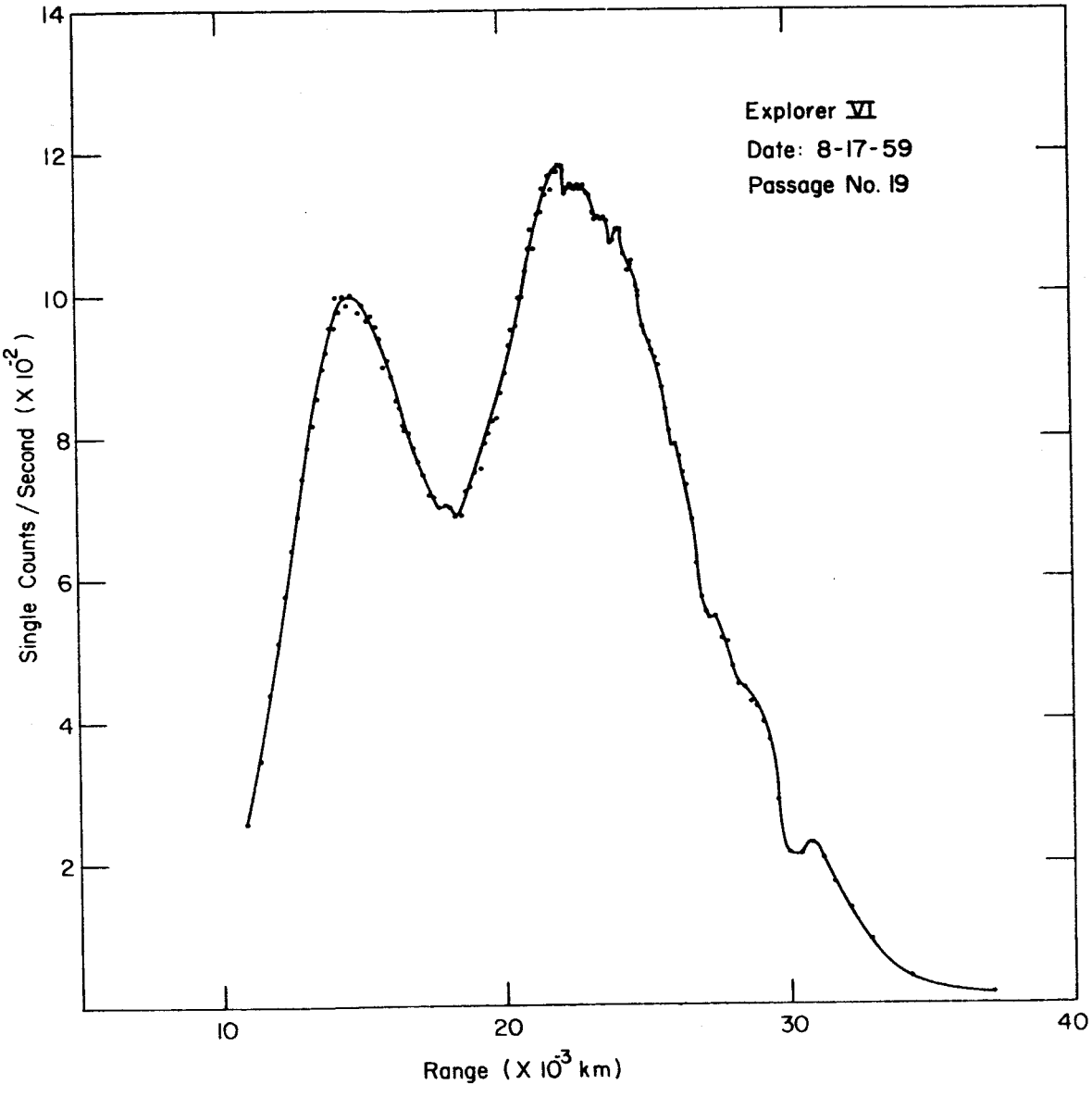
Explorer VI
Date: 8-17-59
Passage No. 19
Single Counts / Second (X 10^-2)
Range (X 10^3 km)
14
12
10
8
6
4
2
10
20
30
40

Figure 7A

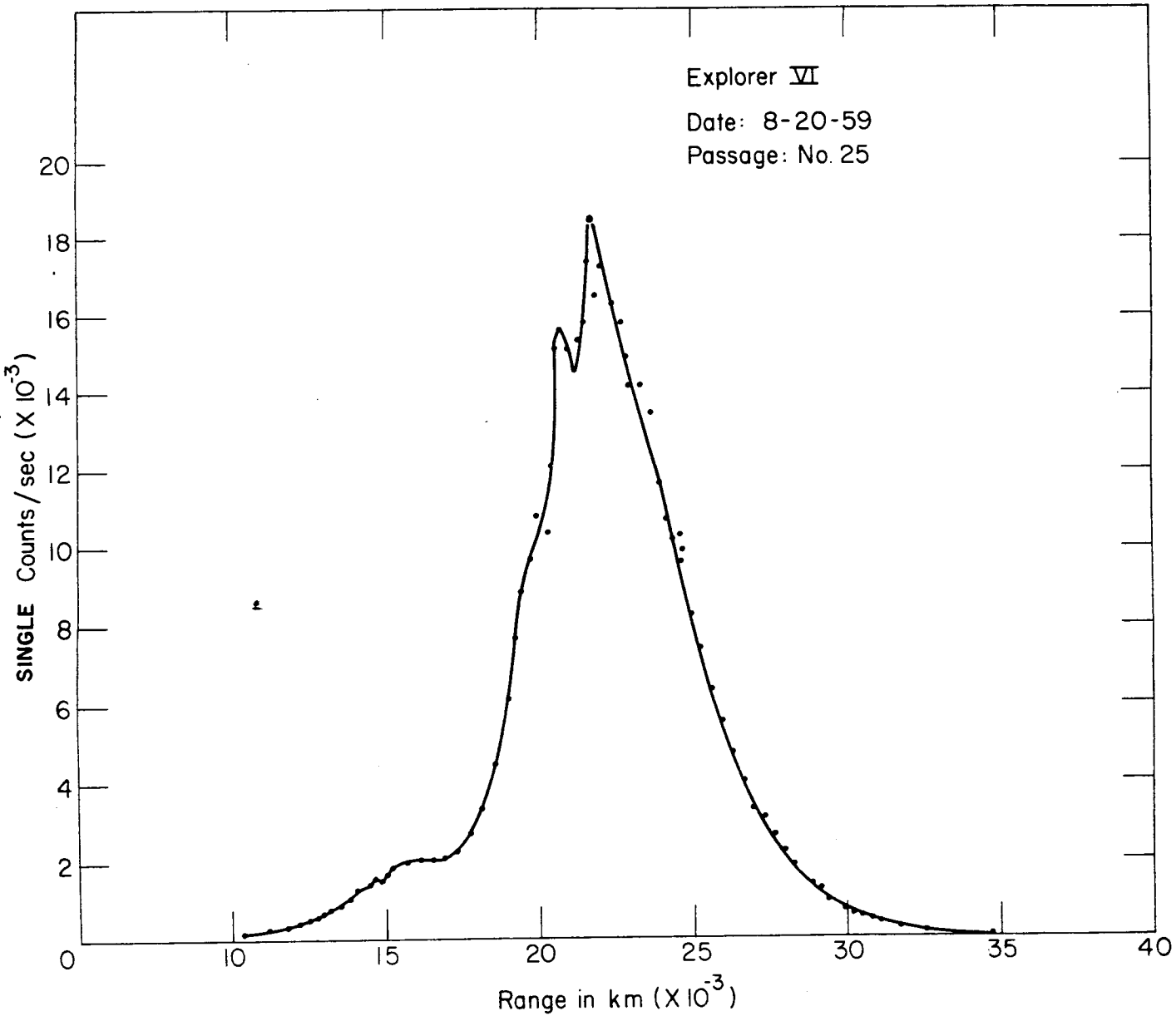
Explorer VI
Date: 8-20-59
Passage: No. 25
SINGLE Counts/sec (X 10^-3)
0
2
4
6
8
10
12
14
16
18
20
10
15
20
25
30
35
40
Range in km (X 10^-3)

Figure 7B

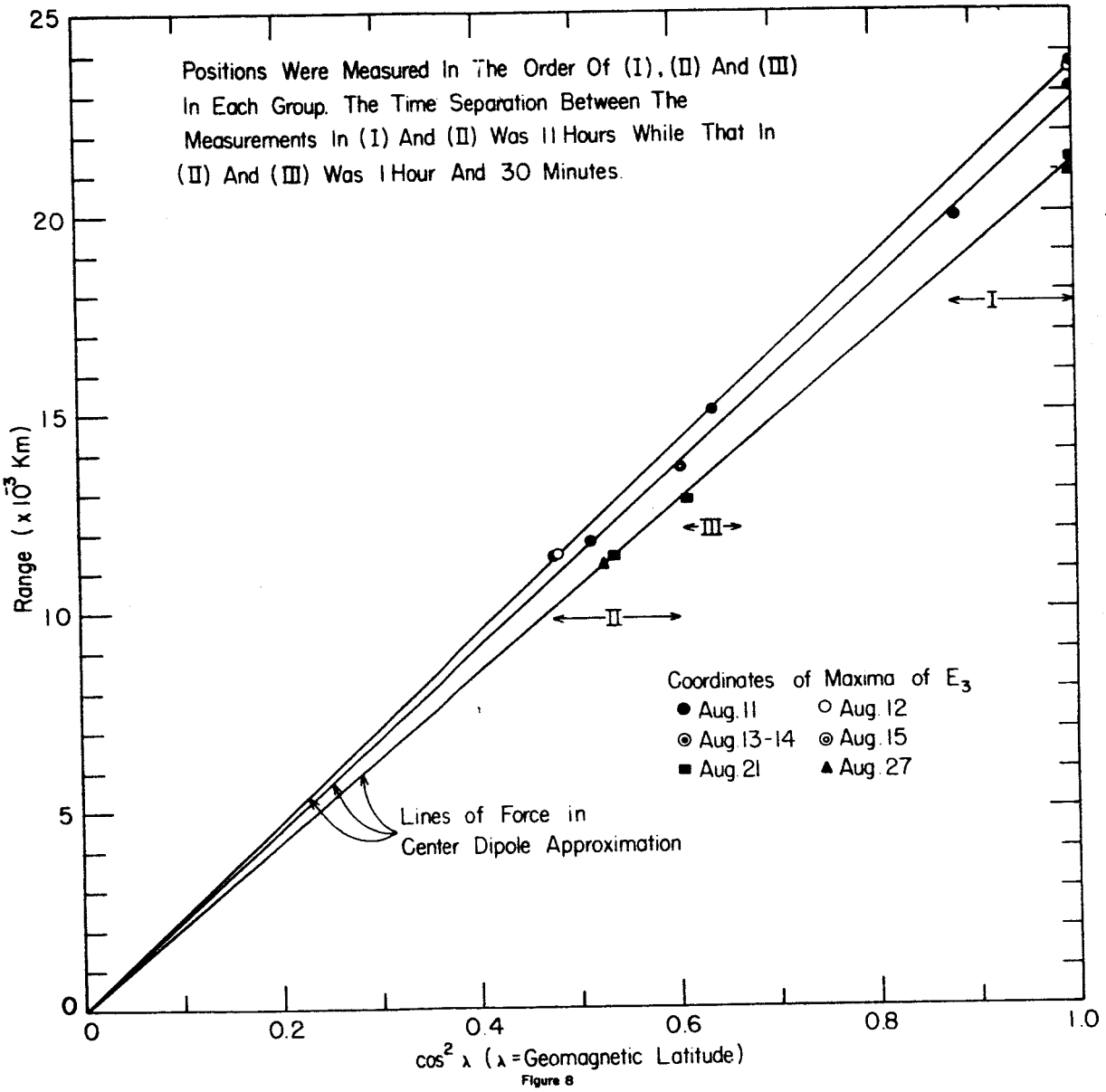
Positions Were Measured In The Order Of (I), (II) And (III) In Each Group. The Time Separation Between The Measurements In (I) And (II) Was 11 Hours While That In (II) And (III) Was 1 Hour And 30 Minutes.
Range (x 10^-3 Km)
cos^2 λ (λ = Geomagnetic Latitude)
I
II
III
Coordinates of Maxima of E3
Aug. 11
Aug. 12
Aug. 13-14
Aug. 15
Aug. 21
Aug. 27
Lines of Force in Center Dipole Approximation
0
5
10
15
20
25
0.2
0.4
0.6
0.8
1.0

Figure 8

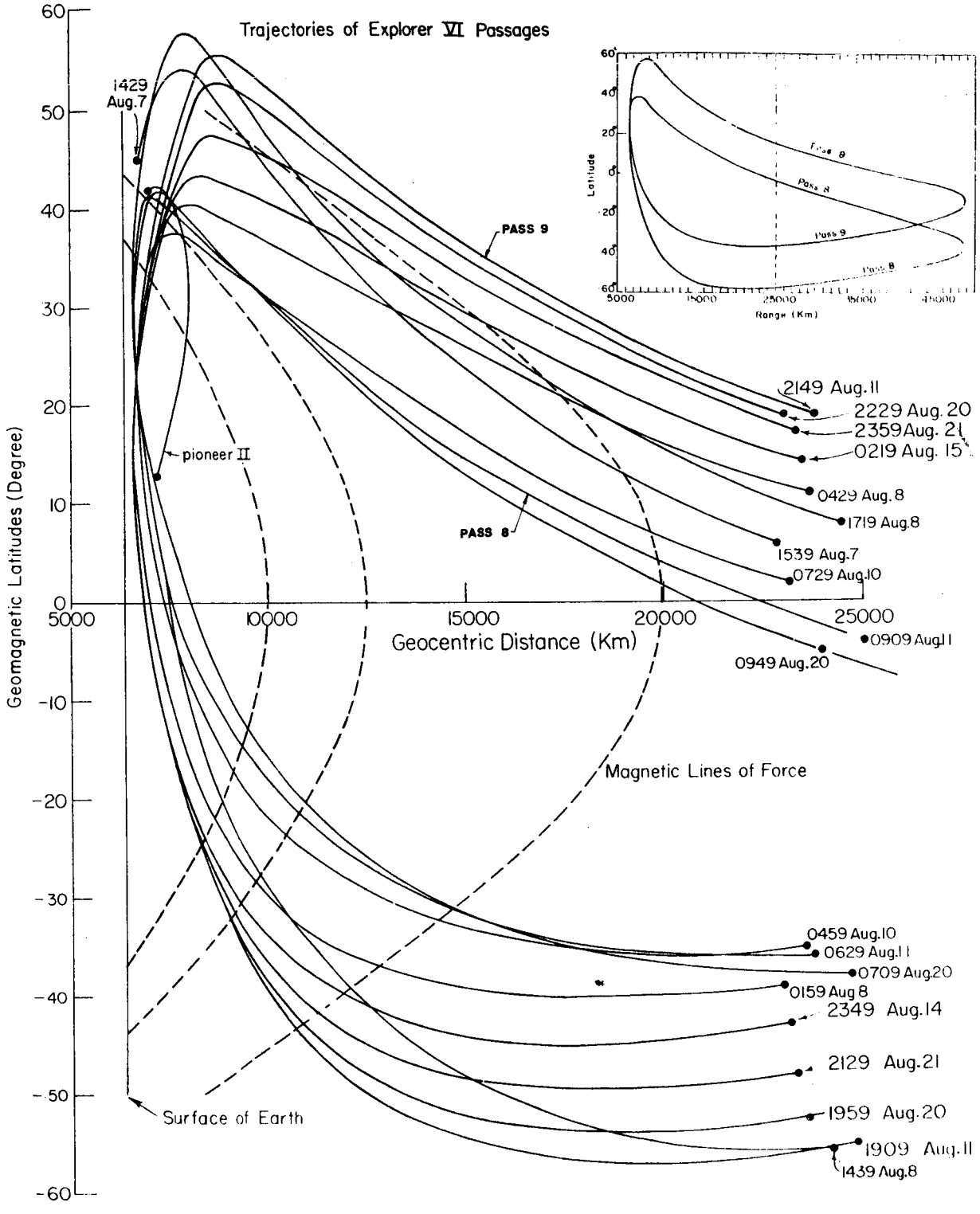
Trajectories of Explorer VI Passages
1429 Aug.7
PASS 9
PASS 8
pioneer II
2149 Aug.11
2229 Aug.20
2359 Aug.21
0219 Aug.15
0429 Aug.8
1719 Aug.8
1539 Aug.7
0729 Aug.10
0909 Aug.11
0949 Aug.20
0459 Aug.10
0629 Aug.11
0709 Aug.20
0159 Aug.8
2349 Aug.14
2129 Aug.21
1959 Aug.20
1909 Aug.11
1439 Aug.8
Magnetic Lines of Force
Surface of Earth
Geomagnetic Latitudes (Degree)
Geocentric Distance (Km)
Latitude
Range (Km)

Figure 9

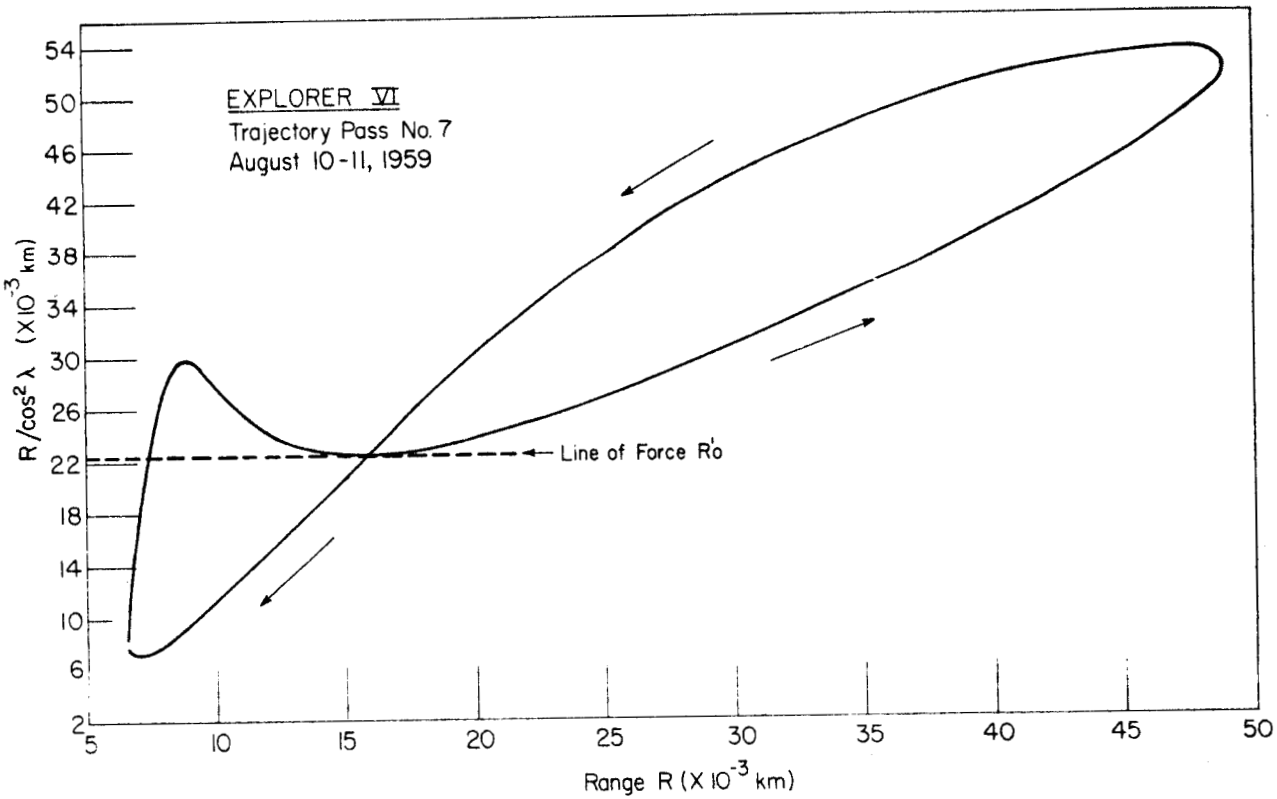
EXPLORER VI
Trajectory Pass No. 7
August 10-11, 1959
Line of Force R'o
R/cos²λ (X10⁻³ km)
Range R (X 10⁻³ km)
54
50
46
42
38
34
30
26
22
18
14
10
6
2
5
10
15
20
25
30
35
40
45
50

Figure 10

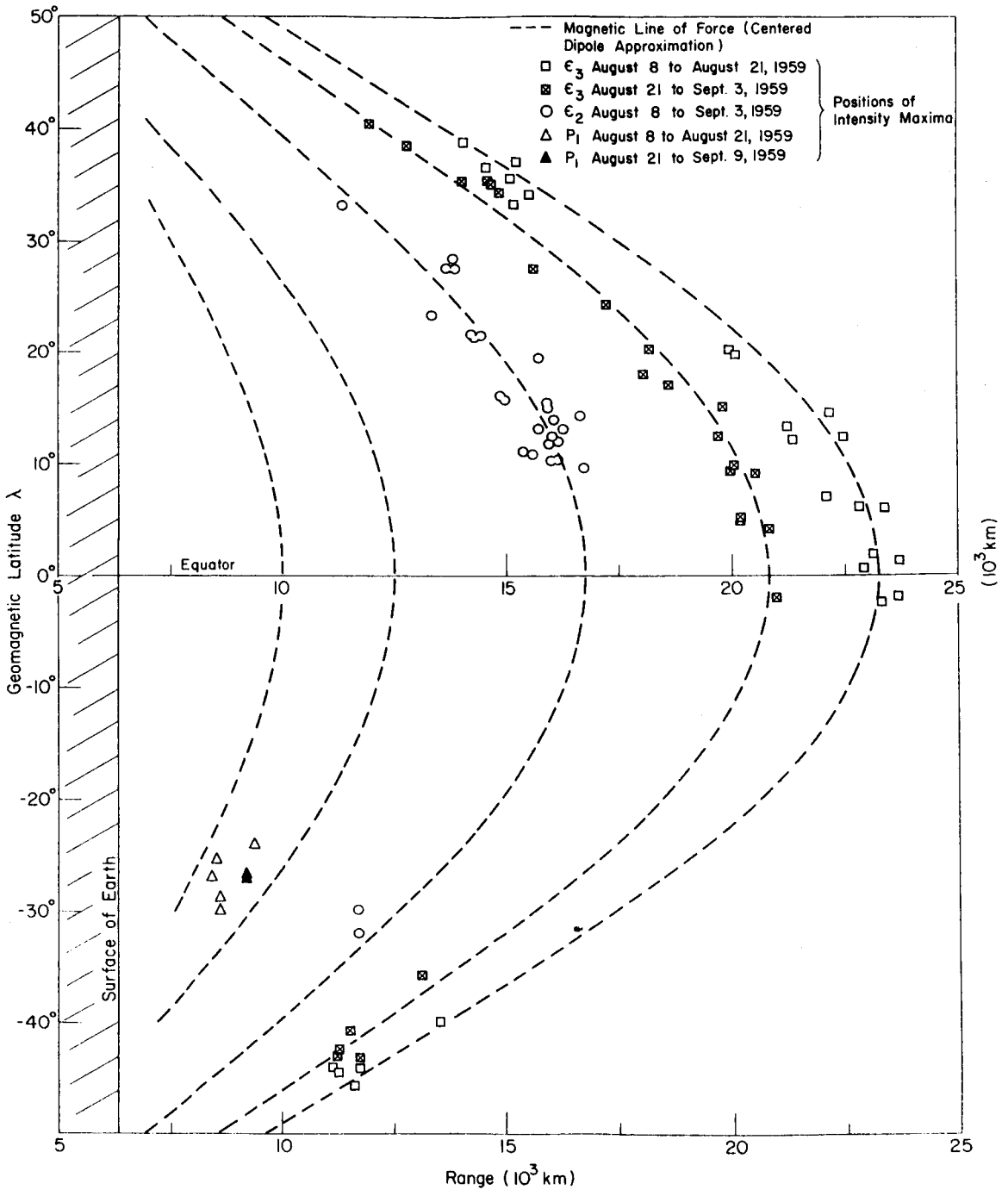
Magnetic Line of Force (Centered Dipole Approximation)
ϵ_3 August 8 to August 21, 1959
ϵ_3 August 21 to Sept. 3, 1959
ϵ_2 August 8 to Sept. 3, 1959
P_1 August 8 to August 21, 1959
P_1 August 21 to Sept. 9, 1959
Positions of Intensity Maxima
Equator
Surface of Earth
Geomagnetic Latitude λ
Range (10^3 km)
(10^3km)
50°
40°
30°
20°
10°
0°
-10°
-20°
-30°
-40°
5
10
15
20
25

Figure 11

Explorer VI
August 7 — October 6, 1959

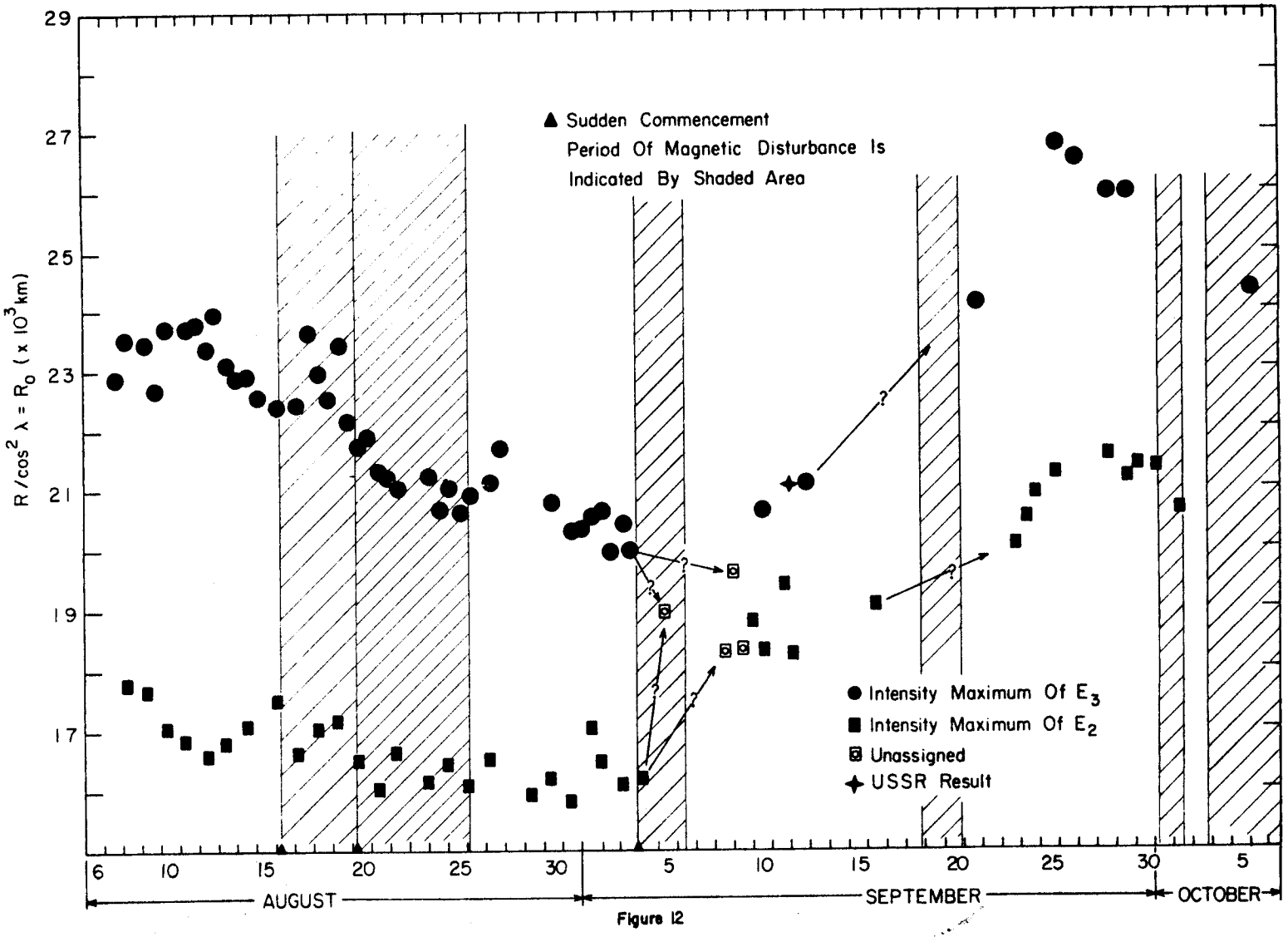

Figure 12

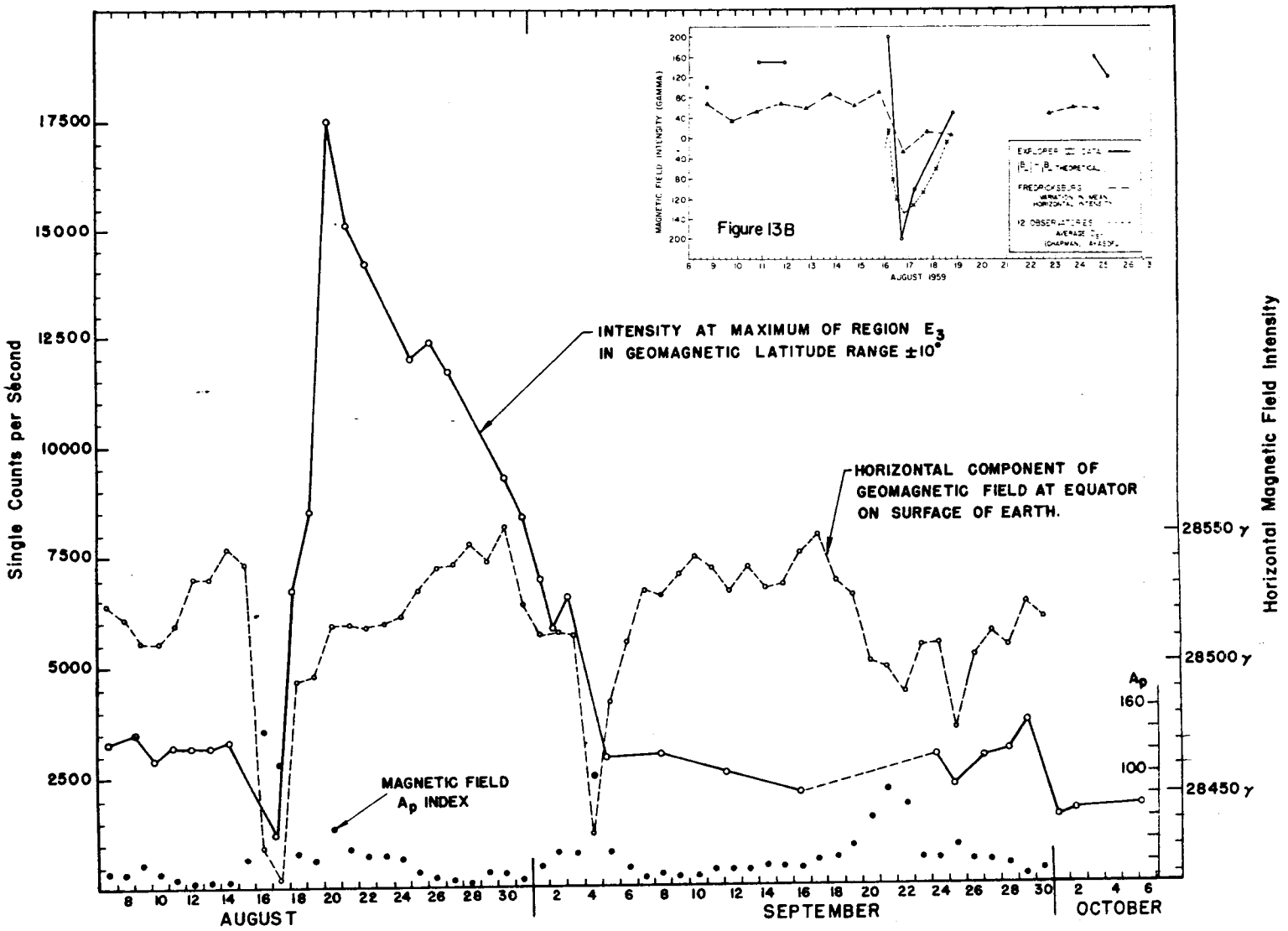
Single Counts per Second
17500
15000
12500
10000
7500
5000
2500
INTENSITY AT MAXIMUM OF REGION E_3
IN GEOMAGNETIC LATITUDE RANGE ±10°
HORIZONTAL COMPONENT OF
GEOMAGNETIC FIELD AT EQUATOR
ON SURFACE OF EARTH.
MAGNETIC FIELD
A_p INDEX
A_p
160
100
28550 γ
28500 γ
28450 γ
Horizontal Magnetic Field Intensity
8 10 12 14 16 18 20 22 24 26 28 30
AUGUST
2 4 6 8 10 12 14 16 18 20 22 24 26 28 30
SEPTEMBER
2 4 6
OCTOBER
1959
Figure 13B
AUGUST 1959

Figure 13A

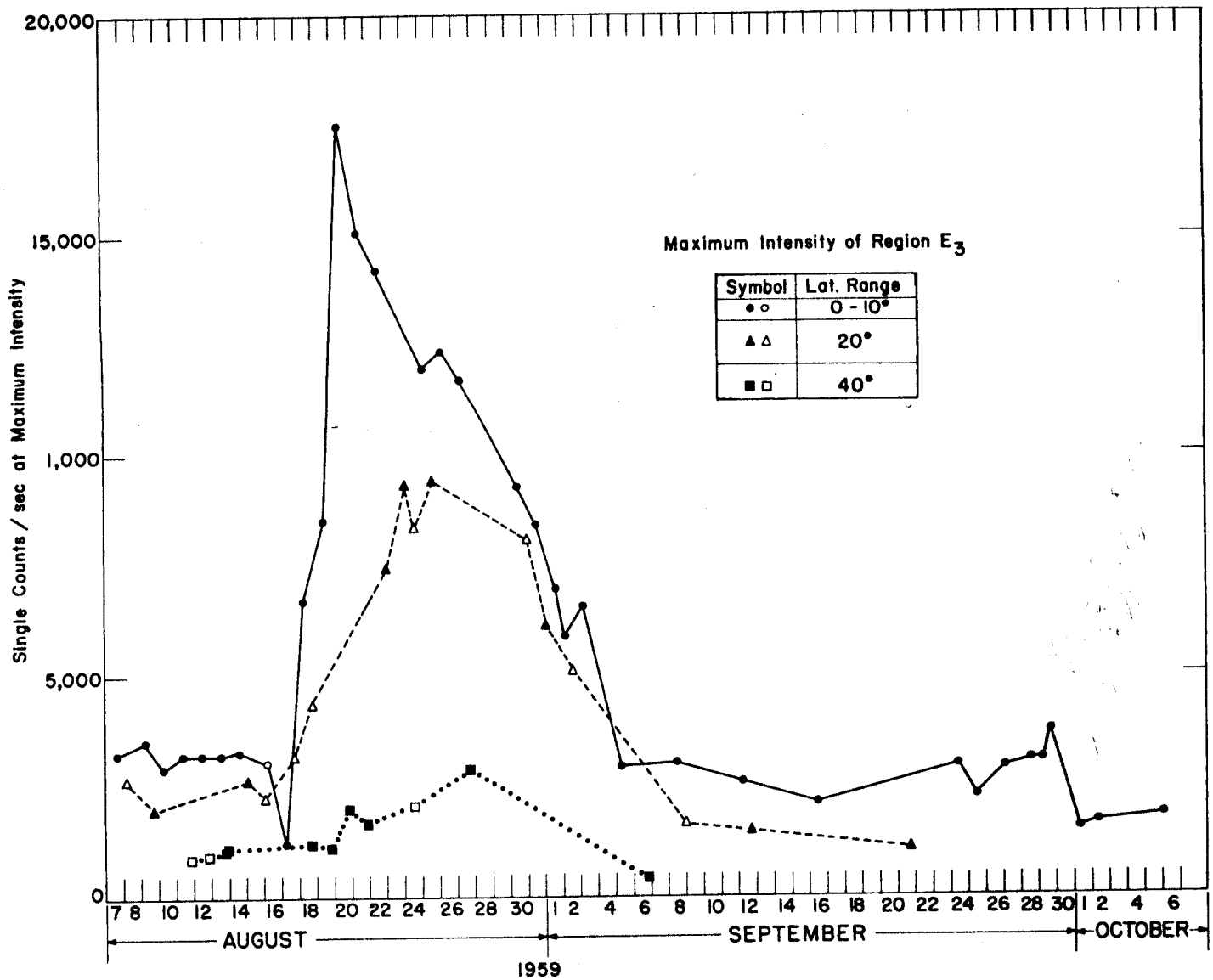
20,000
15,000
1,000
5,000
0
Single Counts / sec at Maximum Intensity
Maximum Intensity of Region E_3
Symbol
Lat. Range
0 - 10°
20°
40°
7 8 10 12 14 16 18 20 22 24 26 28 30 1 2 4 6 8 10 12 14 16 18 20 22 24 26 28 30 1 2 4 6
AUGUST
SEPTEMBER
OCTOBER
1959

Figure 14

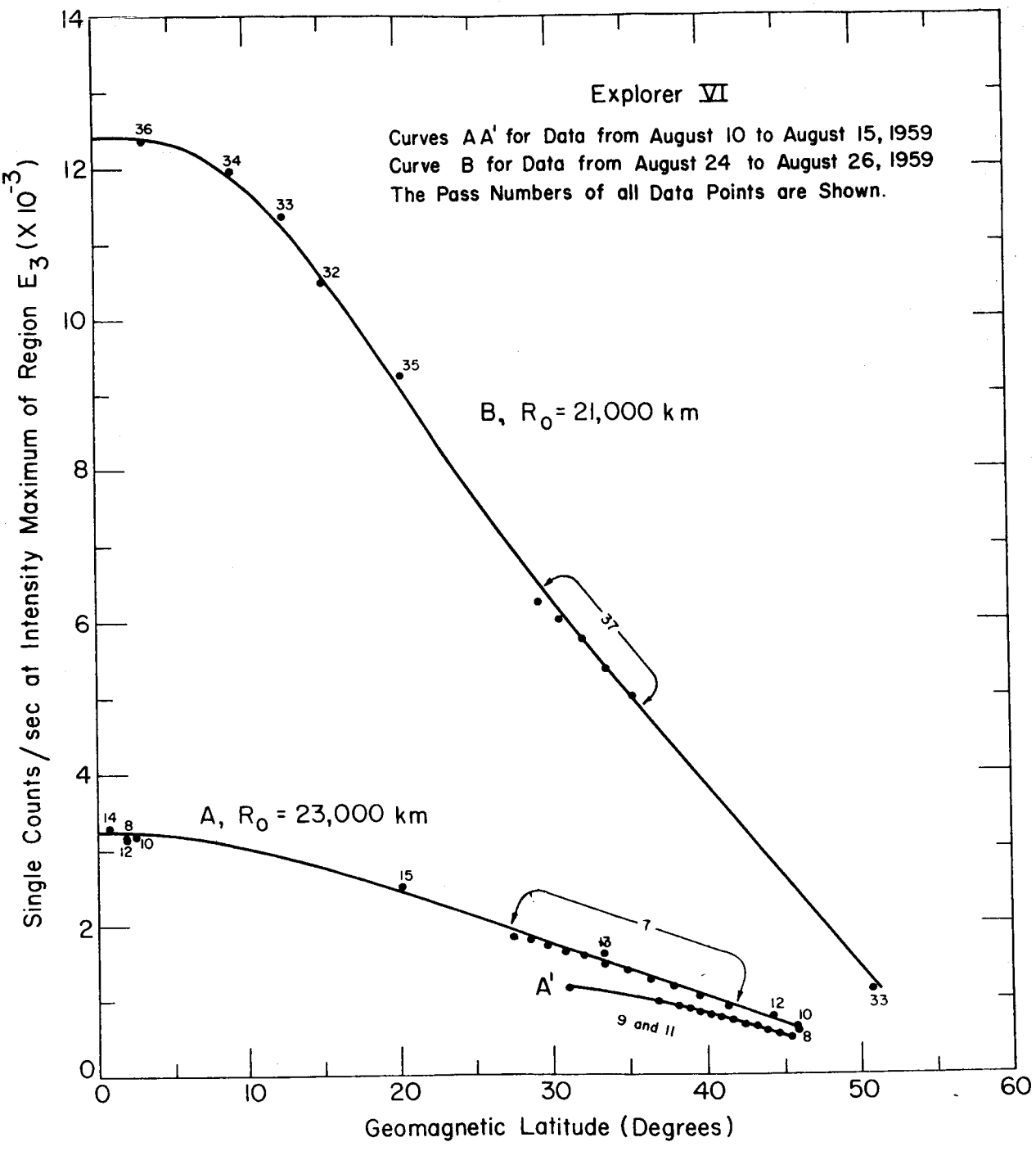
Explorer VI
Curves A A' for Data from August 10 to August 15, 1959
Curve B for Data from August 24 to August 26, 1959
The Pass Numbers of all Data Points are Shown.
B, R_0 = 21,000 km
A, R_0 = 23,000 km
A'
9 and 11
Single Counts / sec at Intensity Maximum of Region E_3 ($\times 10^{-3}$)
Geomagnetic Latitude (Degrees)
0
2
4
6
8
10
12
14
0
10
20
30
40
50
60

Figure 15

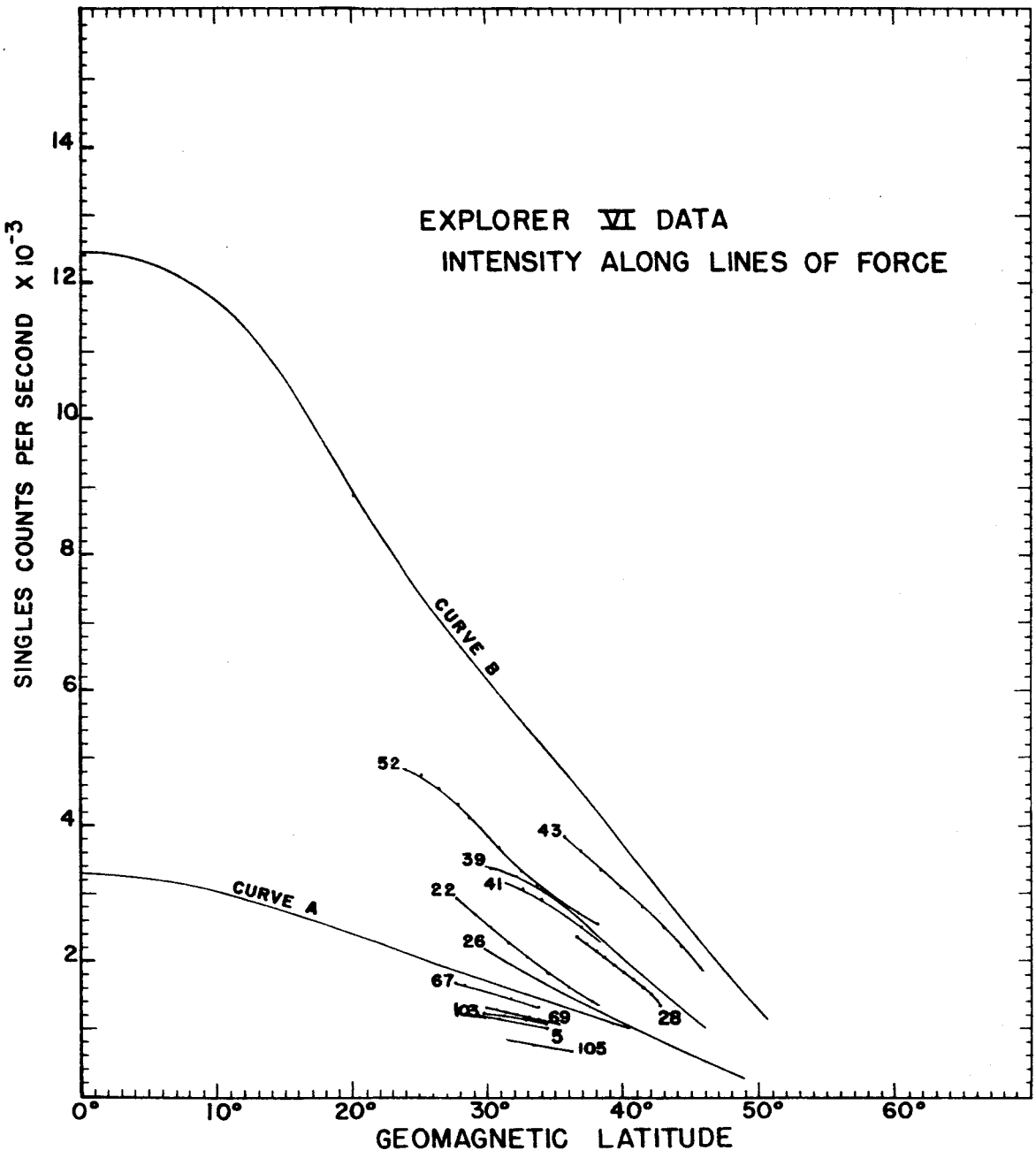
EXPLORER VI DATA
INTENSITY ALONG LINES OF FORCE
SINGLES COUNTS PER SECOND X 10⁻³
GEOMAGNETIC LATITUDE
0°
10°
20°
30°
40°
50°
60°
2
4
6
8
10
12
14
CURVE A
CURVE B
52
43
39
41
22
26
67
103
69
28
5
105

Figure 16

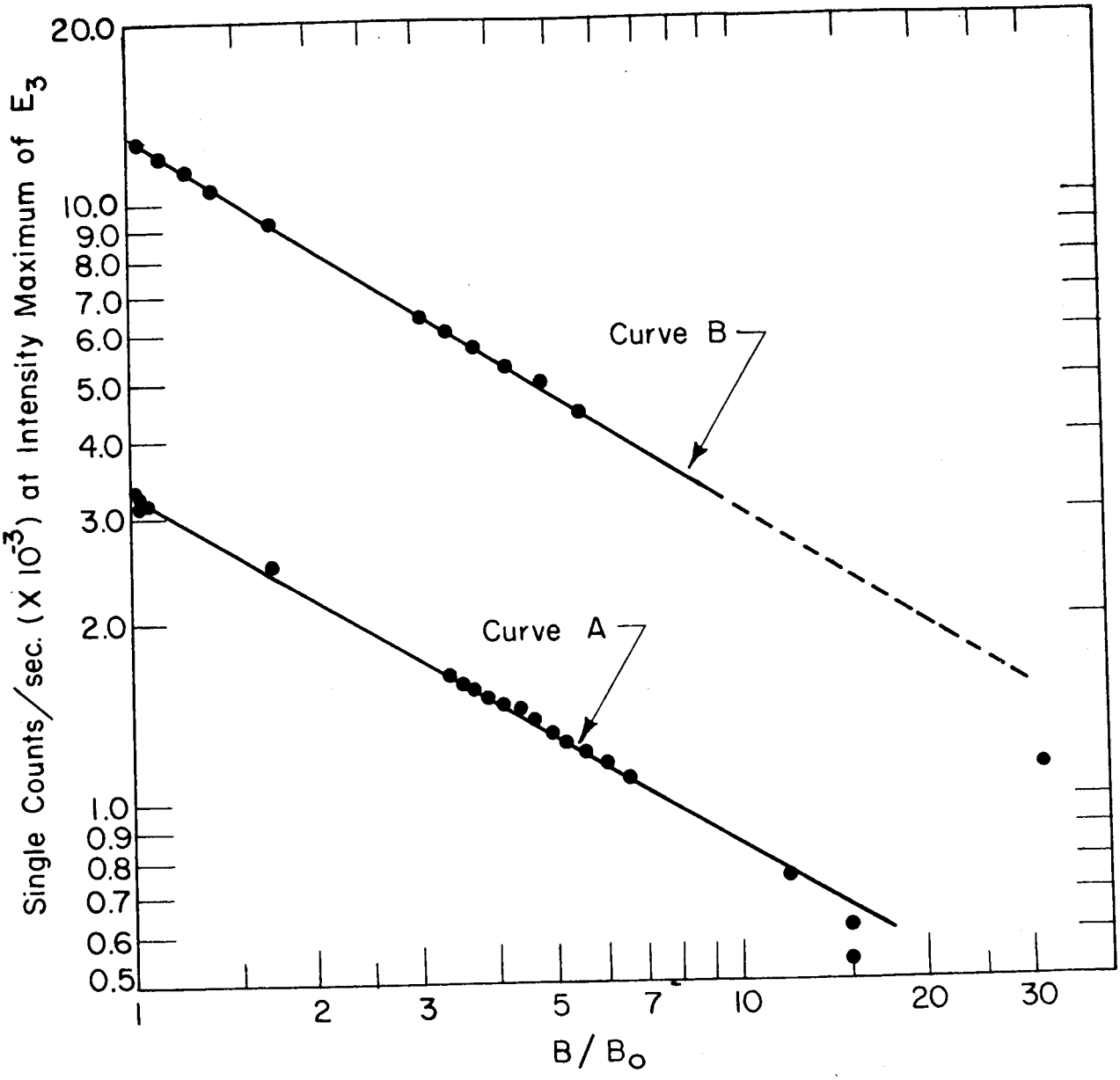
20.0
10.0
9.0
8.0
7.0
6.0
5.0
4.0
3.0
2.0
1.0
0.9
0.8
0.7
0.6
0.5
Single Counts/sec. (X 10^{-3}) at Intensity Maximum of E_3
Curve B
Curve A
1
2
3
5
7
10
20
30
B/ B_o

Figure 17

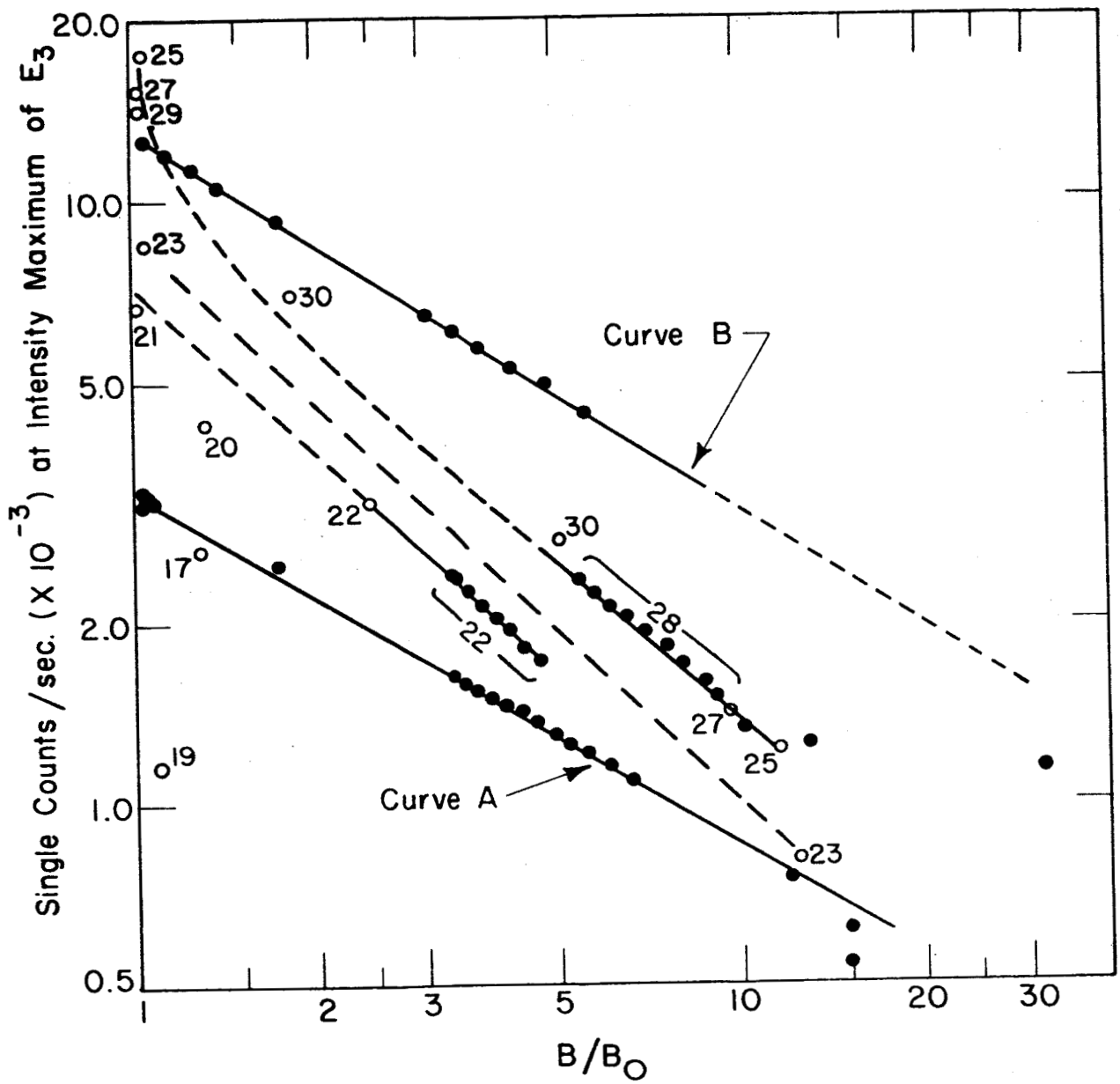
Single Counts /sec. (X 10^{-3}) at Intensity Maximum of E_3
20.0
10.0
5.0
2.0
1.0
0.5
1
2
3
5
10
20
30
B/B_O
o25
o27
o29
o23
o30
o21
o20
22°
o30
17°
28
22
27
25
o19
Curve A
Curve B
o23

Figure 18

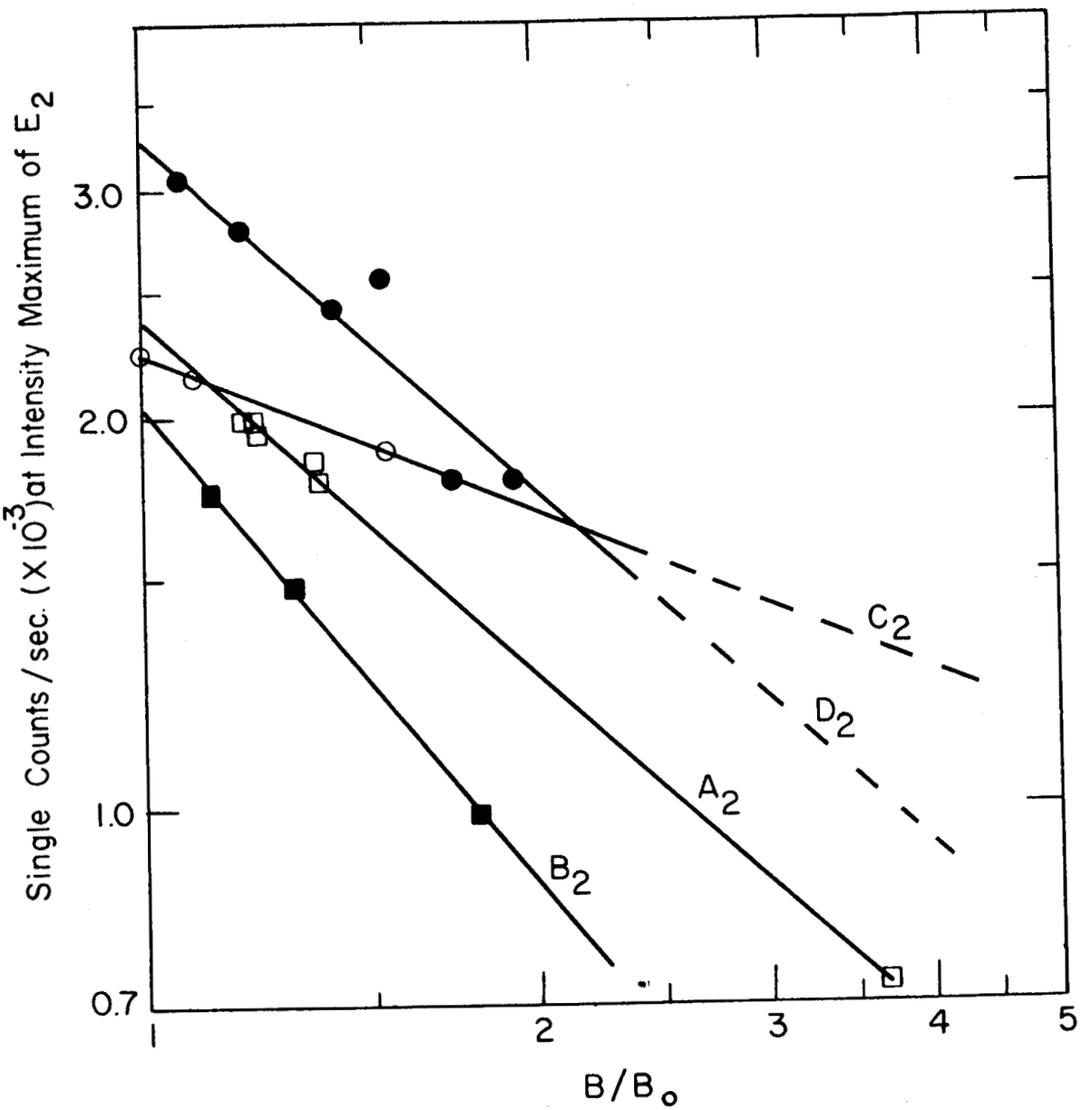
Single Counts / sec. (X 10^-3) at Intensity Maximum of E2
3.0
2.0
1.0
0.7
1
2
3
4
5
B/Bo
C2
D2
A2
B2

Figure 19

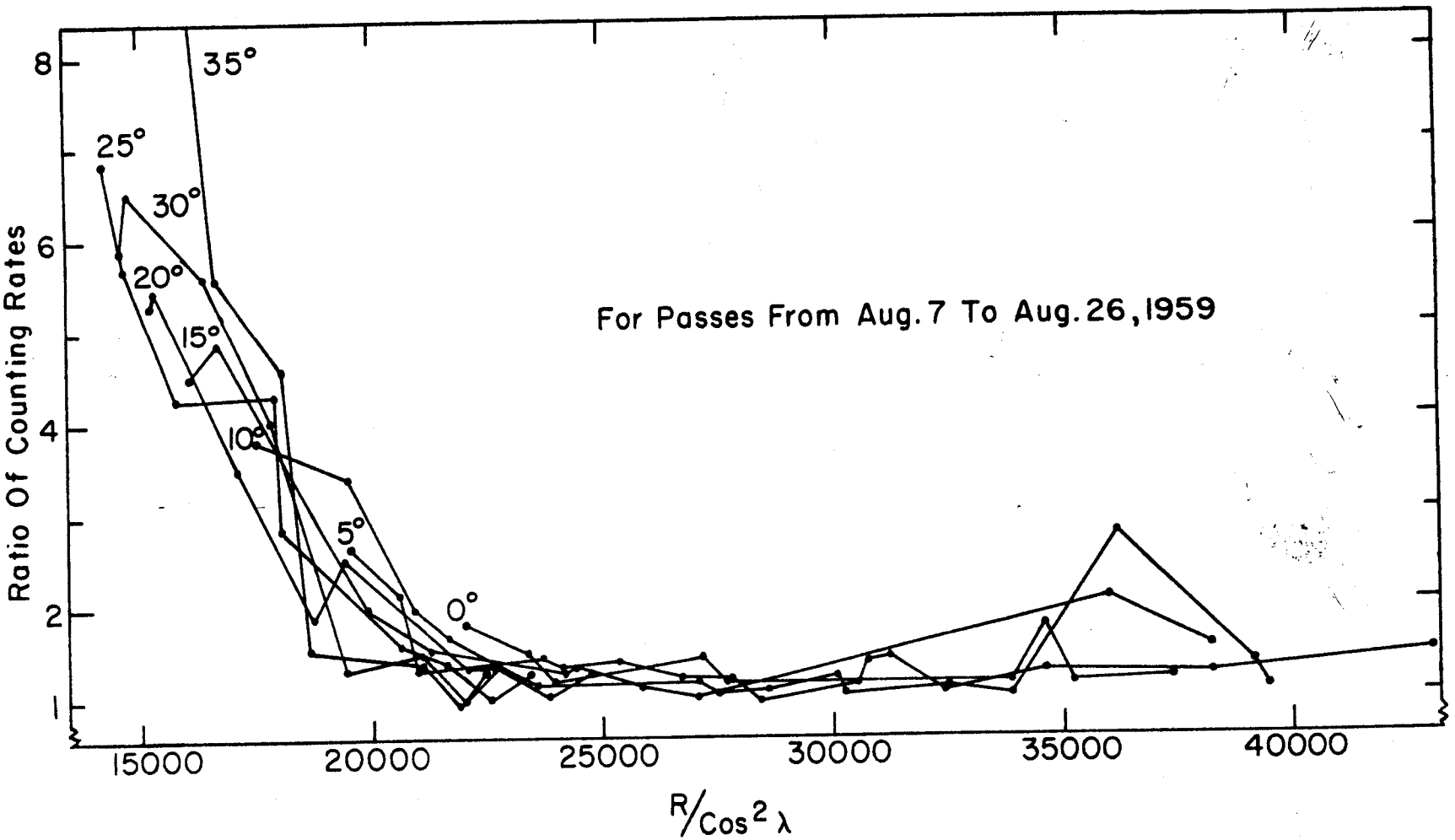
35°
25°
30°
20°
15°
10°
5°
0°
For Passes From Aug. 7 To Aug. 26, 1959
Ratio Of Counting Rates
8
6
4
2
1
15000
20000
25000
30000
35000
40000
R/Cos² λ
Range In Kilometers At Geomagnetic Equator

Figure 20

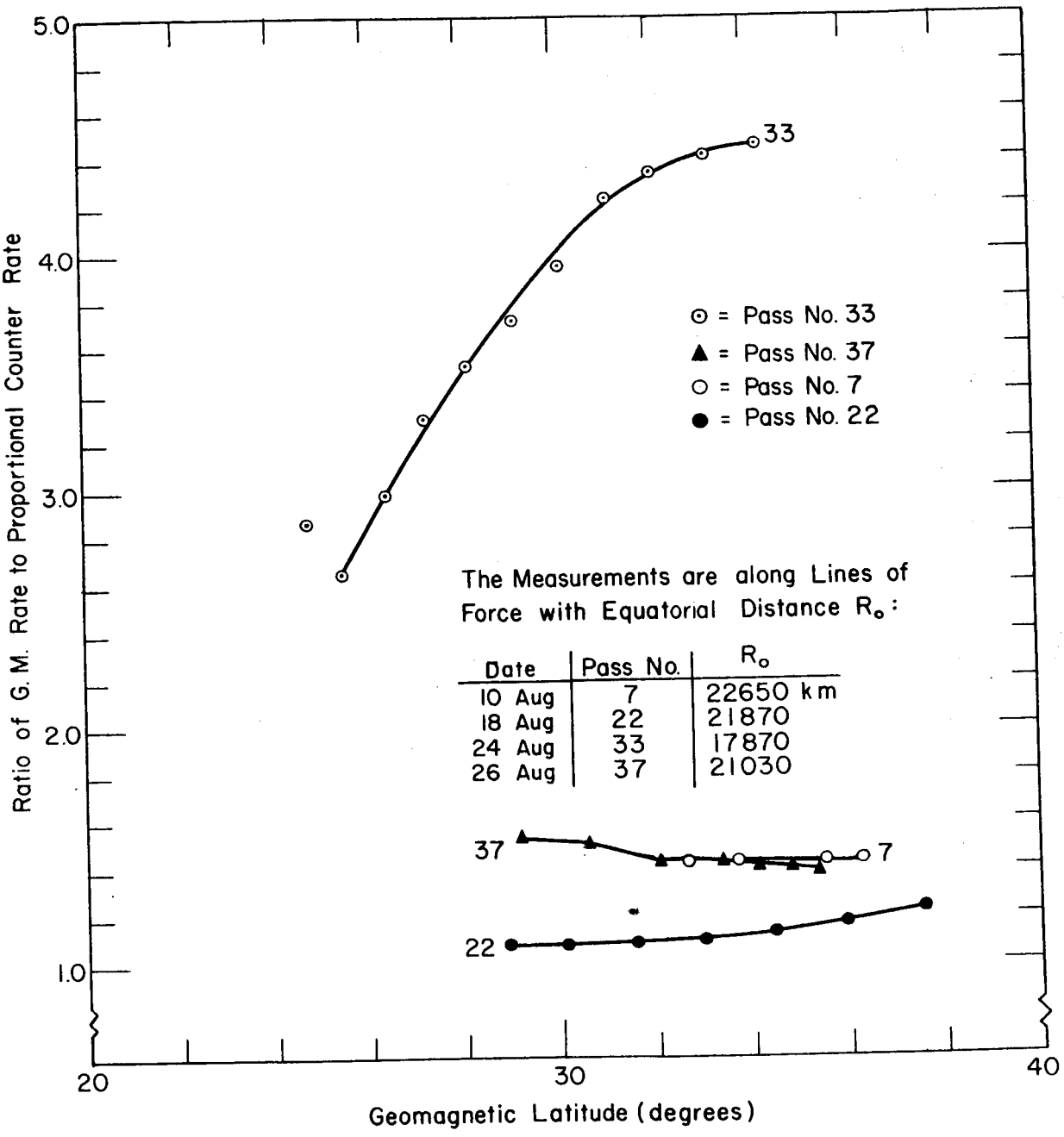
5.0
4.0
3.0
2.0
1.0
Ratio of G.M. Rate to Proportional Counter Rate
20
30
40
Geomagnetic Latitude (degrees)
33
37
7
22
⊙ = Pass No. 33
▲ = Pass No. 37
○ = Pass No. 7
● = Pass No. 22
The Measurements are along Lines of Force with Equatorial Distance R_o:
Date | Pass No. | R_o
10 Aug | 7 | 22650 km
18 Aug | 22 | 21870
24 Aug | 33 | 17870
26 Aug | 37 | 21030

Figure 21

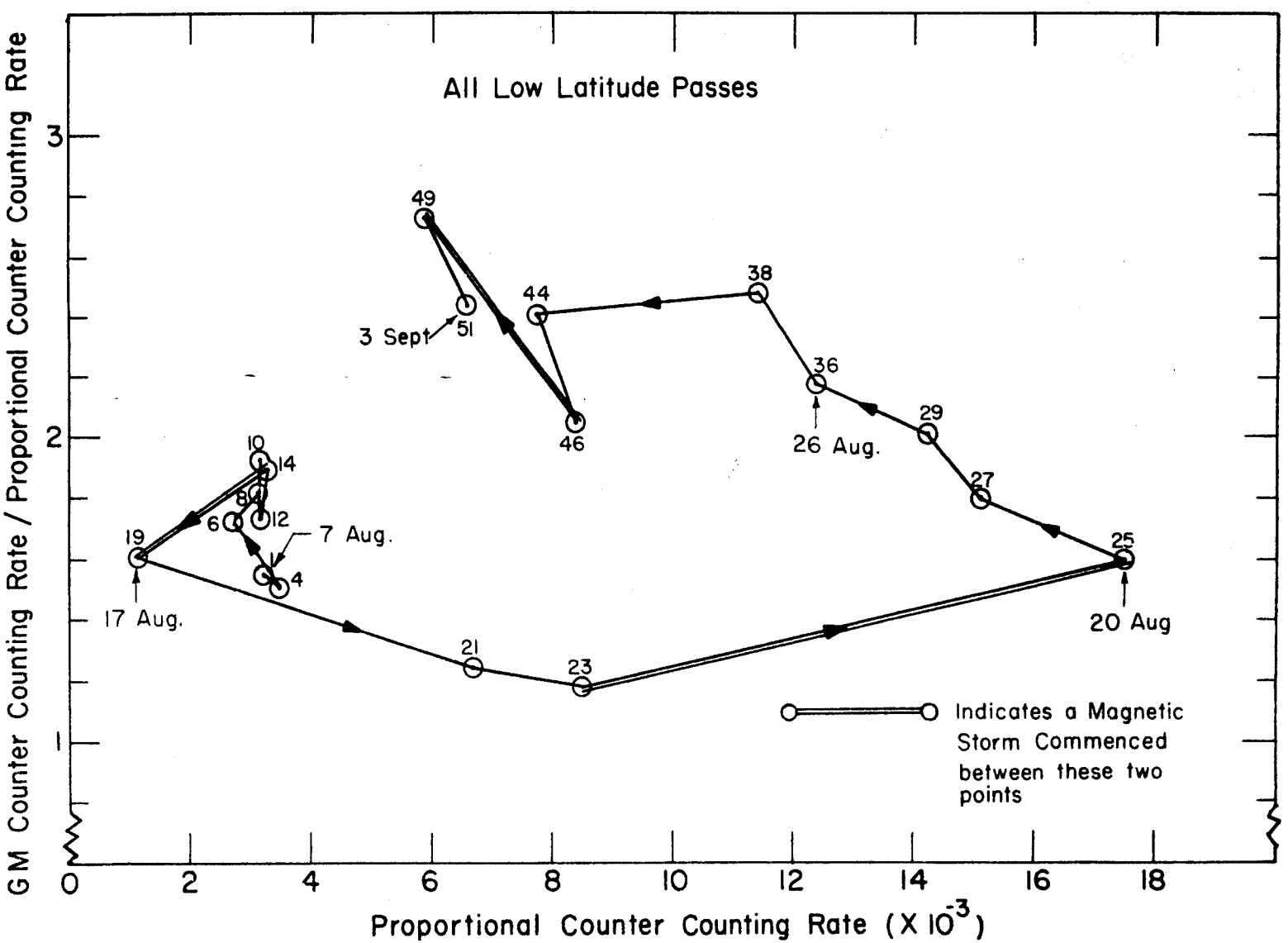
All Low Latitude Passes
GM Counter Counting Rate / Proportional Counter Counting Rate
Proportional Counter Counting Rate (X 10⁻³)
0
2
4
6
8
10
12
14
16
18
1
2
3
49
51
3 Sept
44
46
38
36
26 Aug.
29
27
25
20 Aug
10
14
8
6
12
7 Aug.
19
4
17 Aug.
21
23
Indicates a Magnetic Storm Commenced between these two points

Figure 22

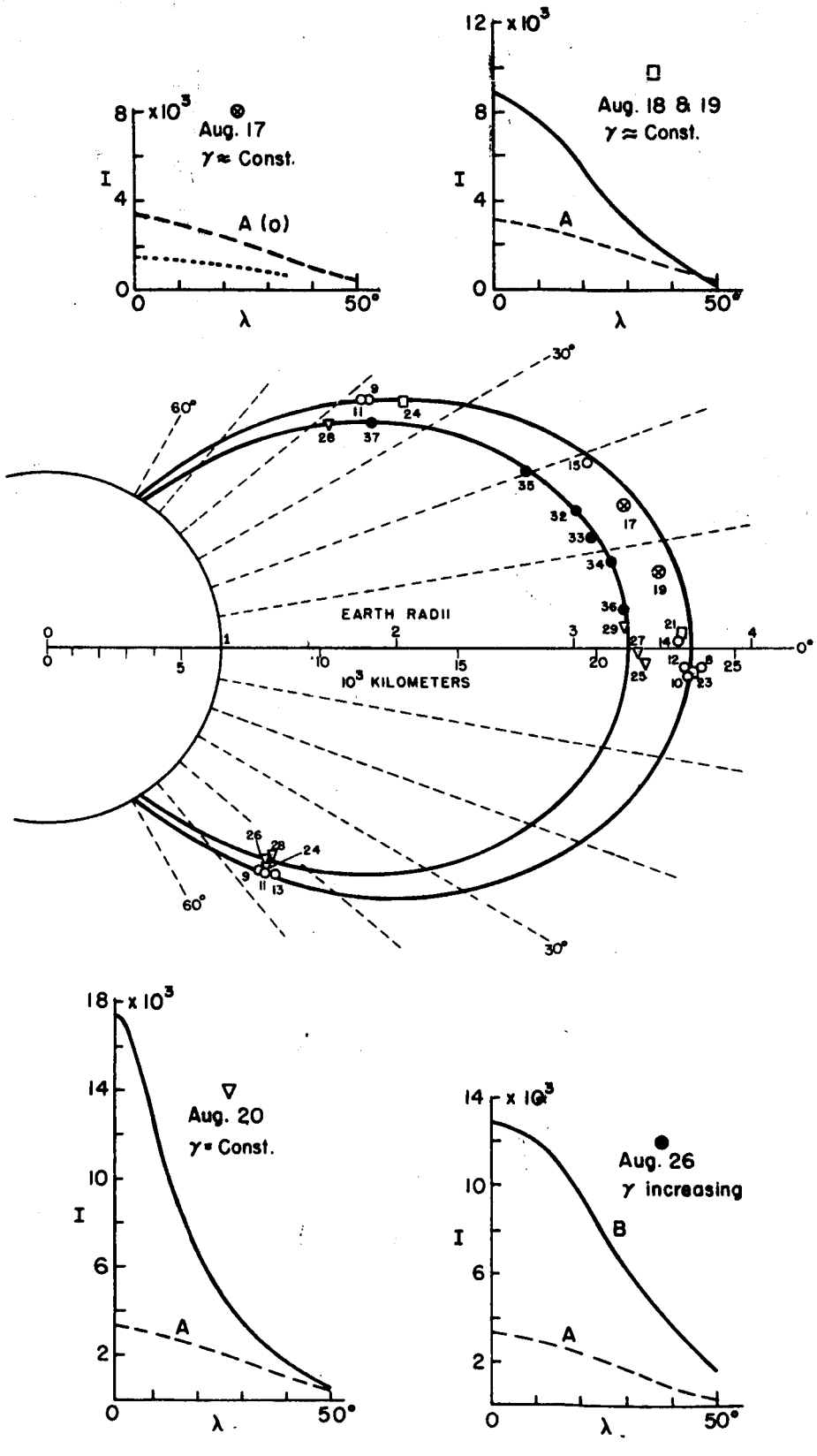

These Data Are For The Maximum Intensity Of The E_3 Region

Figure 23

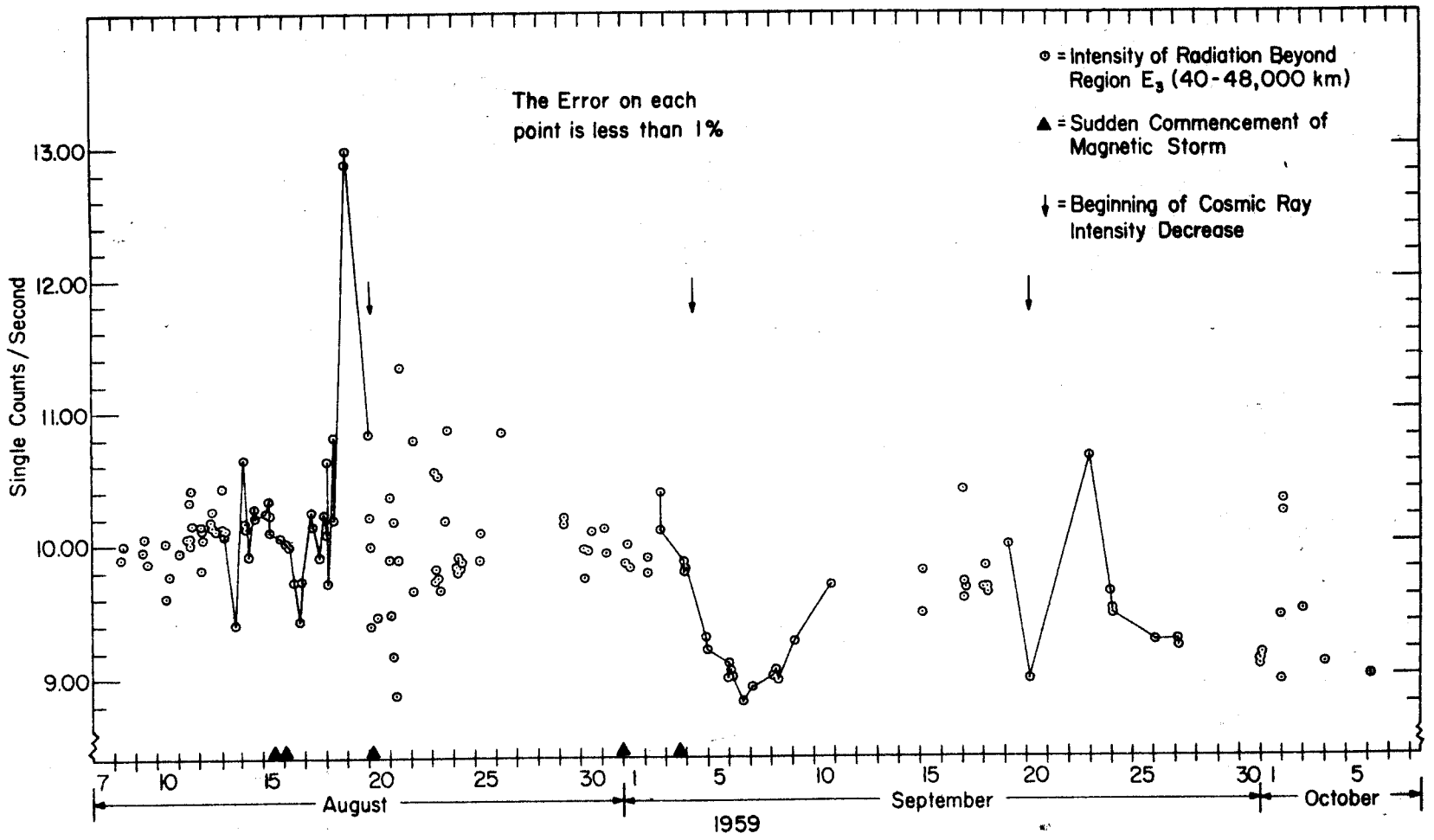
⊙ = Intensity of Radiation Beyond Region E_3 (40-48,000 km)
▲ = Sudden Commencement of Magnetic Storm
↓ = Beginning of Cosmic Ray Intensity Decrease
The Error on each point is less than 1%
Single Counts / Second
13.00
12.00
11.00
10.00
9.00
7
10
15
20
25
30
1
5
10
15
20
25
30
1
5
August
September
October
1959

Figure 24

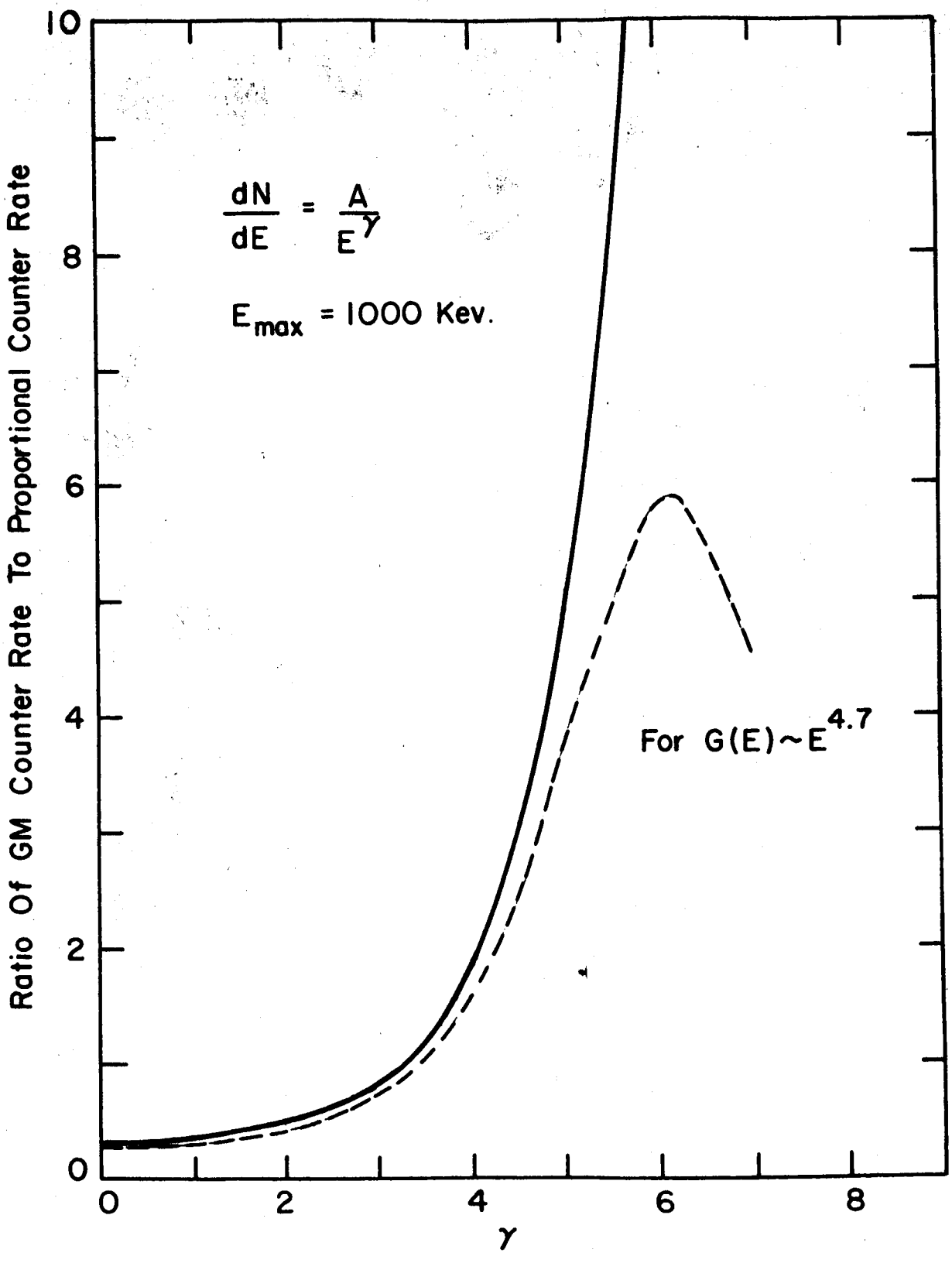
Ratio Of GM Counter Rate To Proportional Counter Rate
10
8
6
4
2
0
0
2
4
6
8
γ
$\frac{dN}{dE} = \frac{A}{E^{\gamma}}$
E_{max} = 1000 Kev.
For $G(E) \sim E^{4.7}$

Figure 25